

**PURDUE UNIVERSITY
GRADUATE SCHOOL
Thesis/Dissertation Acceptance**

This is to certify that the thesis/dissertation prepared

By Ahmed Mohammed Alotaibi

Entitled
DEVELOPMENT OF A MECHATRONICS INSTRUMENT ASSISTED SOFT TISSUE MOBILIZATION (IASTM) DEVICE
TO QUANTIFY FORCE AND ORIENTATION ANGLES

For the degree of Master of Science in Mechanical Engineering

Is approved by the final examining committee:

Sohel Anwar

Chair

Mary T. Loghmani

Stanley Yung-Ping Chien

To the best of my knowledge and as understood by the student in the Thesis/Dissertation Agreement, Publication Delay, and Certification Disclaimer (Graduate School Form 32), this thesis/dissertation adheres to the provisions of Purdue University's "Policy of Integrity in Research" and the use of copyright material.

Approved by Major Professor(s): Sohel Anwar

Approved by: Sohel Anwar 4/19/2016
Head of the Departmental Graduate Program Date

DEVELOPMENT OF A MECHATRONICS INSTRUMENT ASSISTED SOFT
TISSUE MOBILIZATION (IASTM) DEVICE TO QUANTIFY FORCE AND
ORIENTATION ANGLES

A Thesis

Submitted to the Faculty

of

Purdue University

by

Ahmed Mohammed Alotaibi

In Partial Fulfillment of the

Requirements for the Degree

of

Master of Science in Mechanical Engineering

May 2016

Purdue University

Indianapolis, Indiana

I would like to dedicate this work to my parents, wife, sisters, brother and children.

ACKNOWLEDGMENTS

I would like to thank Dr. Sohel Anwar for his support, guidance and encouragement throughout my masters thesis work. In addition, I express my appreciation to Dr. Mary T. Loghmani and Dr. Stanley Yung-Ping Chien for their suggestions and comments during my research.

I would like to thank Fabian Lischke for his help with 3D printing. In addition, I express my appreciation to Bruce Neff, Samantha Rose Bane and Allison Danielle Longgood from the School of Health and Rehabilitation Science for their contributions and feedback in the testing stage of this thesis.

Finally, I would like to thank my parents, wife, sisters, brother and children for their love and support.

TABLE OF CONTENTS

	Page
LIST OF TABLES	vi
LIST OF FIGURES	vii
ABSTRACT	x
1 Introduction	1
1.1 Problem Statement	1
1.2 Literature Review	2
1.3 Objective	5
2 PROPOSED IASTM TOOL DESIGNS	6
2.1 Design Requirements	6
2.2 Electronic Component Selection	6
2.3 1D Compression Load Cell Based Design	8
2.4 3D Load Cell Based Design	13
2.4.1 Labview Model Building for 3D Load Cell Device	21
2.5 IASTM Tool Fabrication Using 3D Printing Technology	24
3 FINITE ELEMENT ANALYSIS OF THE PROPOSED DESIGNS	27
3.1 Modeling Initialization	27
3.1.1 Skin and Tissue Modeling	27
3.1.2 IASTM Modeling	30
3.1.3 Simulation Scenarios Setup	33
3.2 Analysis Results and Discussion	41
3.2.1 Frictional Scenario	41
3.2.2 Bonded Scenario	48
4 MEASUREMENTS VALIDATION TEST	54
4.1 Validation Systems	54

	Page
4.1.1 Force Validation System	54
4.1.2 Angle Validation System	57
4.2 Methodology and Test Results	57
4.3 IASTM Device Dynamic Analysis	62
5 CONCLUSION AND FUTURE WORK	64
5.1 Conclusion	64
5.2 Future Work Recommendation	65
LIST OF REFERENCES	66
APPENDICES	
A 3D LOAD CELL DATA SHEET	69
B ARDUINO CODE FOR ANGLE MEASUREMENT (FREE IMU-YAW- PITCH-ROLL)	70
B.1 Code 90 Degrees	70
B.2 Code 360 Degrees	71
C SCALE DATA SHEET	73

LIST OF TABLES

Table	Page
2.1 Resultant Forces on Skin with Different Orientation Angles Under 100N Compression Force	20
3.1 Mechanical Properties of Human Skin	28
3.2 Mechanical Properties of the Compression IASTM Load Cell Device . .	31
3.3 Initial Information for IASTM Device Simulation Using Contacts Areas	36
3.4 Hand Pressure on the Back of Device in FEA (Frictional Connection) .	39
3.5 Initial Information for AISTM Device Simulation Using Contacts Areas	40
3.6 Hand Pressure on the Back of Device in FEA (Bonded Connection) . .	42
4.1 Summary of The Scale Accuracy Test	55
4.2 Scale Data Format	56
4.3 Summary of The First Force Measurement Test	58
4.4 Summary of The Second Force Measurement Test	59
4.5 Summary of The Third Force Measurement Test	60
4.6 Summary Pitch Angle Measurement Test	62

LIST OF FIGURES

Figure	Page
1.1 Graston Technique® Instrument Set	1
1.2 GT-3 Treatment tip [13]	5
2.1 IMUduino microcontroller [22]	7
2.2 The Smallest Compression Load Cell (FC-08) [23]	7
2.3 The 3D load cell	8
2.4 The External Amplifier for the 3D Load Cell	8
2.5 Device Based on the Compression Load Cell	9
2.6 Tip Design for the Device Based on the Compression Load Cell	9
2.7 Sensor Placements for the Compression Load Cell Model	10
2.8 Back Cover of the Compression Load Cells Device	10
2.9 Mechatronic IASTM Device Orientation Angles and Sensors Placement.	11
2.10 Force Analysis for 90-degree Force Applied to the Tool	12
2.11 Force Analysis for 0-89 Degrees Force Applied to the Tool	12
2.12 Force Analysis for 91-180 Degrees Force Applied to the Tool	13
2.13 Full Section for the Compression Load Cell Device	13
2.14 3D Load Cell Device	14
2.15 3D Load Cell Device Frame Parts	14
2.16 3D Load Cell Device Tip	15
2.17 3D Load Cell Device Back Cover	15
2.18 Half Section of the 3D Load Cell Device	16
2.19 Main Coordinates for the 3D Load Cell Device	17
2.20 Final Coordinates for the 3D Load Cell Device	17
2.21 3D Load Cell Device System Configuration	21
2.22 Force Measurement Labview Model for the 3D Load Cell Design	22

Figure	Page
2.23 Orientation Measurement Labview Model for the 3D Load Cell Design	23
2.24 The IASTM Measurements Labview Model	25
2.25 The IASTM Device Front Panel	26
2.26 3D Printed Model of Compression Load Cell Device	26
2.27 3D Printed Model of 3D Load Cell Device	26
3.1 Human Arm Model in ANSYS	28
3.2 Skin Meshing	29
3.3 Compression IASTM Load Cell Device in ANSYS	30
3.4 Compression Load Cell Embedded into the Device Tail	31
3.5 Meshed Load Cell Device	32
3.6 Meshed Load Cell Tail	32
3.7 Device Tail Bonded Connection	33
3.8 Device Tip Bonded Connection	34
3.9 Skin Frictional Contact Area	35
3.10 Device Tip Frictional Contact Areas	35
3.11 Direction of Devices Acceleration	37
3.12 Device Displacement Constraint Areas	37
3.13 Applied Force to IASTM Device on the Tool Neck	38
3.14 Applied Force to IASTM Device on the Back Cover	38
3.15 Device Displacement Constraint Areas	41
3.16 Force Convergence Chart (Frictional Connection)	43
3.17 Hand Pressure vs. Equivalent Stress on Skin (Frictional Connection)	44
3.18 Maximum Equivalent Stress under Hand Pressure of 0.20 MPa (Frictional Connection)	44
3.19 Maximum Principal Stress on Skin vs. Hand Pressure (Frictional Connection)	45
3.20 Maximum Value of the Maximum Principal Stress Under Hand Pressure of 0.25 MPa (Frictional Connection)	45
3.21 Skin Total Deformation (Frictional Connection)	46

Figure	Page
3.22 Maximum Total Deformation (4.0012 mm) Under Hand Pressure 0.25 MPa (Frictional Connection)	46
3.23 Maximum Four Load Cells Stress Distribution vs. hand pressure (Frictional Connection)	47
3.24 Minimum Four Load Cells Stress Distribution vs. Hand Pressure (Frictional Connection)	48
3.25 Hand Force vs. Equivalent Stress on Skin (Bonded Connection)	49
3.26 Maximum Equivalent Stress under Maximum Hand Force (120 N) (Bonded Connection)	50
3.27 Maximum Principal Stress on Skin vs. Hand Force (Bonded Connection)	50
3.28 Maximum Value of the Maximum Principal Stress Under Maximum Hand Force (120 N) (Bonded Connection)	51
3.29 Skin Total Deformation (Bonded Connection)	51
3.30 Maximum Total Deformation Under Hand Force 120 N	52
3.31 Maximum Four Load Cells' Stress Distribution vs. Hand Force	53
3.32 Minimum Four Load Cells' Stress Distribution vs. Hand Pressure	53
4.1 Electronic Scale	54
4.2 Scale Labview Model	56
4.3 Combination Square Set (Angle Validation System)	57
4.4 Hand Position of IASTM Device in the First and Second Tests	58
4.5 Hand Position of IASTM Device in the Third Test	60
4.6 IASTM Device at 30 Degrees	61
4.7 IASTM Device at 45 Degrees	61
4.8 IASTM Device at 60 Degrees	61
4.9 Summary of the Dynamic Test for the IASTM Device	63
4.10 Stroke Number During the Dynamic Test	63
Appendix Figure	
A.1 3D Load Cell Data Sheet	69
C.1 Scale Data Sheet	73

ABSTRACT

Alotaibi, Ahmed Mohammed. M.S.M.E., Purdue University, May 2016. Development of a Mechatronics Instrument Assisted Soft Tissue Mobilization (IASTM) Device to Quantify Force and Orientation Angles. Major Professor: Sohel Anwar.

Instrument assisted soft tissue mobilization (IASTM) is a form of massage using rigid manufactured or cast devices. The delivered force, which is a critical parameter in massage during IASTM, has not been measured or standardized for most clinical practices. In addition to the force, the angle of treatment and frequency play an important role during IASTM. As a result, there is a strong need to characterize the delivered force to a patient, angle of treatment, and stroke frequency.

This thesis proposes two novel mechatronic designs for a specific instrument from Graston Technique®(Model GT3), which is a frequently used tool to clinically deliver localized pressure to the soft tissue. The first design is based on compression load cells, where 4-load cells are used to measure the force components in three-dimensional space. The second design uses a 3D load cell, which can measure all three force components simultaneously. Both designs are implemented with IMUduino microcontroller chips which can also measure tool orientation angles and provide computed stroke frequency.

Both designs, which were created using Creo CAD platform, were also analyzed thoroughly for strength and integrity using the finite element analysis package ANSYS. Once the static analysis was completed, a dynamic model was created for the first design to simulate IASTM practice using the GT-3 tool. The deformation and stress on skin were measured after applying force with the GT-3 tool. Additionally, the relationship between skin stress and the load cell measurements has been investigated. The second design of the mechatronic IASTM tool was validated for force

measurements using an electronic plate scale that provided the baseline force values to compare with the applied force values measured by the tool. The load cell measurements and the scale readings were found to be in agreement within the expected degree of accuracy. The stroke frequency was computed using the force data and determining the peaks during force application. The orientation angles were obtained from the built-in sensors in the microchip.

1. INTRODUCTION

1.1 Problem Statement

Physical therapy has been used to help people to relieve their pains and stresses for thousands of years. The physical therapy practice has different styles and methods, which have been improved and modified to meet patients satisfaction and wellbeing. Instrument assisted soft tissue mobilization (IASTM) is a massage technique that uses solid tools to enhance the restricted tissue. In 1994, Graston Technique® introduced a massage methodology based on IASTM using six different tools for different tasks and functions, illustrated in Figure 1.1.



Fig. 1.1. Graston Technique® Instrument Set

Massage therapy has been used widely for decades; however, the lack of force quantification, which can potentially be computed by a physician, has affected the development of optimal dosing during an IASTM process and the understanding of the

underlying biological mechanisms [1–3]. The IASTM has offered interesting results with different conditions and tissues [4–11]. These studies showed that the force applied by the therapist is a critical parameter in the IASTM, and it should be quantified and measured accurately for research purposes as well as clinical applications.

1.2 Literature Review

The Graston Technique was introduced to the world of physical therapy by an athlete who had debilitating knee injury during water skiing. Because of the insufficiency of Physical therapy and surgery at that time; he created different tools to treat his knee's soft tissue using his knowledge in machining. After he succeed on his knee treatment, he decided to work with Ball Memorial Hospital and Ball State University to advance and produce the Graston Technique to the world. In 1994, TherapyCare Resources Inc., which was the main company of Graston Technique, established in Indianapolis [12]. It has been recommended for use on superficial and fibrous structures and in the treatment of soft tissue injury (tendinopathies, triggerpoints, hypertonicity, and myofascial pain). Scar tissue from injury causes pain and restriction of motion-range and functioning in the affected muscles [13].

Instrument assisted soft tissue mobilization (IASTM or ISTM) technique has been utilized in treatment of soft tissue dysfunction. The method focuses on a controlled magnitude of micro-trauma to an area of excessive scar tissue or fibrosis. This has been found to stimulate repair and reorganization of affected tissue [14]. In a study by Heinecke, Thuesen, and Stow [15], the effect of the Graston Technique (GT) was found to better facilitate treatment of soft tissue limitations, when compared with dynamic stretching and strengthening protocols. The GT effect improved shoulder motion in overhead athletes (softball, baseball, or volleyball).

Laudner, et.al [16], argued that due to the repetitive rotational and distractive forces exerted on the posterior shoulder during the deceleration phase of the overhead throwing motion, limited glenohumeral (GH) range of motion (ROM) occurred,

causing shoulder injuries. It was determined that utilization of instrument-assisted soft tissue mobilization (IASTM), such as the Graston Technique, was proven to be effective for various injuries and disorders.

In a case study by Loghmani [17], of a 55-year-old man who had injured the proximal interphalangeal joint of the left index-finger, physical measures were improved, including an immediate gain in finger range of motion with IASTM alone. However, it was seen that manual therapy approaches integrating IASTM could provide an effective conservative treatment strategy for patients with finger-hand conditions in the performing arts and other patient populations.

As a conservative approach, eccentric strengthening exercises have been used for the treatment of Achilles tendinopathy. The recommended treatment period for this approach is 12 weeks. Phipps et. al. [14], demonstrate the potential effectiveness of IASTM as a manual therapy approach for the treatment of tendon disorders. They show the potential to yield positive outcomes in a reduced treatment time. However, it was seen that the treatment regimen included exercise; therefore, the effect of IASTM cannot be isolated. However, despite this limitation, the treatment combination yielded positive outcomes in relatively fewer visits. Looney, et. al. [8] also carried out studies to demonstrate that patients with plantar fasciitis treated with Graston Instrument Soft Tissue Mobilization techniques (GT) and a home stretching program experienced clinically meaningful improvements.

Arthrofibrosis of the knee is a surgical complication that can limit range of motion, inhibit muscle activity, and decrease patient function. In studies by Black [18], the Graston Technique was used as a rehabilitative course in arthrofibrotic limitations. Clear improvement in range of motion and quadriceps activity and function was noted.

Several human and animal studies have attempted to measure the delivered pressure using different strategies for different massage sets. An earlier human study by Hsin-Min Lee et al. [19] investigated the effect of transferred friction massage (TFM) on flexor carpi radialis (FCR) motoneuron (MN) pool excitability. They built an electronic system to evaluate the massage rate, momentary pressure and total cu-

mulative pressure. Their system is based on an ultrathin flexible pressure sensor (ConTacts C500) and it is fixed on a thumb of the physician and insulated by plastic glove. However, this system provided an inaccurate measurement for clinical use for several reasons. Any electrical failure in the system can cause harm either to physician or patient since one of its components is directly in contact with the therapists hand. And different therapists have different thumb sizes and softness, which might affect the force measurements.

Recently, an animal study by Qian Wang et al. [20] has developed an automated device that can generate a certain amount of force using a feedback loop. Force can be applied either with compression or transverse force profiles; however, transverse force is not used as a feedback. The device consists of a base, where small animal (rats and rabbits) are held during application, and two movement axes to apply force in the horizontal (X) and vertical (Z) directions. Two-axis force sensors, which are based on piezoresistance, are mounted at the bottom end of the Z-axis, and can measure both compression and tensile forces in the X and Z directions. Different stainless steel tips, which can be fixed on the two-axis force sensors, have been manufactured according to different tissue size. This bulky equipment has provided a useful method to quantify the force delivered to the subject; however, this device is impractical for clinical usage because of its constraints, and neglecting the transverse force will result in inaccurate force readings.

Similarly, another animal study by Hansong Zeng et al. [21], constructed a vertical automated compression device, which used a pneumatic system to apply a certain amount of force on a rabbit. A linear motion control system was used to control the generated force, and a force sensor (Pasco Inc., U.S.) provided the feedback to the device. But this device conflicted with the repeatability and feasibility required in the clinical practice.

1.3 Objective

In this thesis, two proposed designs of mechatronic IASTM tool for localized application of pressure, similar to the treatment tip of GT3, as shown in Figure 1.2 [13], will be presented, analyzed, built, and evaluated. The first design uses 1D compression load cells, where 4 load cells are used to measure the three force components in the 3D space. The second design uses a 3D load cell. The 3D printing technology has been used to fabricate and assemble these models. The primary objective of this work is to design, build, and test an accurate force measurement system for IASTM tool and provide other important parameters, such as the tool orientation angles, stroke frequency, and a full monitoring system using a suitable platform. The design concepts are intended to enable expansion to other shaped treatment tips for dispersive pressure and use on different shaped body parts.



Fig. 1.2. GT-3 Treatment tip [13]

2. PROPOSED IASTM TOOL DESIGNS

2.1 Design Requirements

To design the mechatronic IASTM device, different parameters should be considered in the design stages. From a safety perspective, the new device must run at relatively low voltage to reduce the risk of electric shock. The device should be compact, lightweight, and portable. The new device require measuring forces within 0-155 N, instrument orientation angles, treatment time, and stroke frequency during a session. It is preferred that the new designs be adaptable to fit different IASTM devices. In addition, they have to be durable and reusable because of their frequent usage in clinics, and they must be available at reasonable prices. Finally, the new instrument must have a real time user interface for researchers, students and therapist. These design requirements are crucial at all design stages, from component selection to the manufacturing process.

2.2 Electronic Component Selection

After considering all design requirements, extensive research was conducted to reach the optimal designs that could meet the requirements stated in the previous section. The IMUduino [22] microcontroller was selected to measure the angles and stroke frequency using its Gyro, a 3-Axis Digital Compass IC, and an Accelerometer. As shown in Figure 2.1, the IMUduino board has a small form factor (39.8 mm × 15.72 mm) which helps in reducing the device size.

An extensive and wide-ranging search on force sensors was performed to select the appropriate force sensors for the new IASTM tool designs. As a result, two load

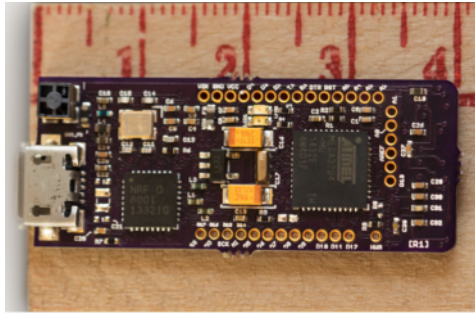


Fig. 2.1. IMUduino microcontroller [22]

cells were selected: the smallest compression load cell and a 3D load cell. Two force measurement strategies were chosen for cost reduction and design versatility purposes.

The first selected force sensor is the smallest compression load cell (FC-08), which is a compression type load cell produced by Forsentek Co., Limited, as shown in Figure 2.2. It can measure up to 20 kg of force acting vertically on its nob with a diameter and height of 8 mm and 5 mm, respectively. Using the compression load cell requires a signal conditioning unit to amplify and filter the output signal.



Fig. 2.2. The Smallest Compression Load Cell (FC-08) [23]

As shown in Figure 2.3, the second load cell is a 3D load cell (USL06-H5-500N-C), which is made by Tec Gihan Co., Ltd. This load cell can measure forces in three dimensional space, with force ranges of up to ± 500 , ± 500 , and $+1000$ N for X, Y and

Z, respectively. An external amplifier (DSA-03A) supplied by the same company was used for signal conditioning, as shown in Figure 2.4.

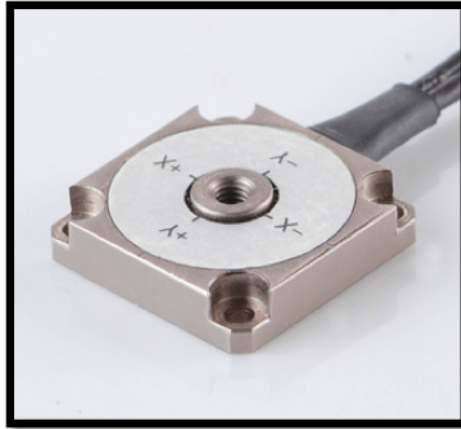


Fig. 2.3. The 3D load cell



Fig. 2.4. The External Amplifier for the 3D Load Cell

2.3 1D Compression Load Cell Based Design

After all electronics and sensors have been selected, the new designs of the IASTM tool were created using Creo Parametric 2.0 CAD software. The first model was constructed based on the compression load cell, as shown in Figure 2.5. This device

consists of four parts: tip, frame, back cover, and keyways. As shown in Figure 2.6, the tip was designed to be similar to the GT-3 tip, so it would have the same precision for targeting soft tissues. A back cavity was designed to fit all electronic component sizes needed for the device, as shown in Figure 2.5. A back cover was used to seal and insulate the electronics inside the cavity, as shown in Figures 2.8. The cross section of the frame was narrowed for finger placements in consideration of the overall diameter and sensor placements.

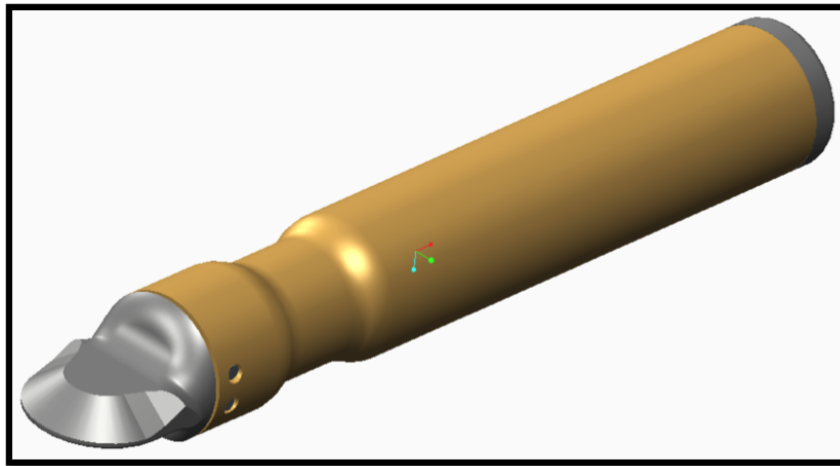


Fig. 2.5. Device Based on the Compression Load Cell

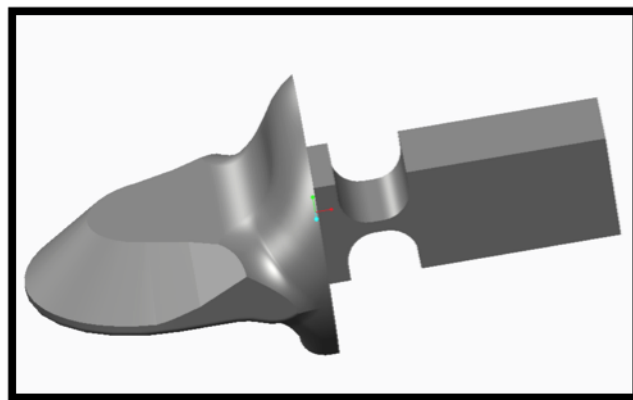


Fig. 2.6. Tip Design for the Device Based on the Compression Load Cell

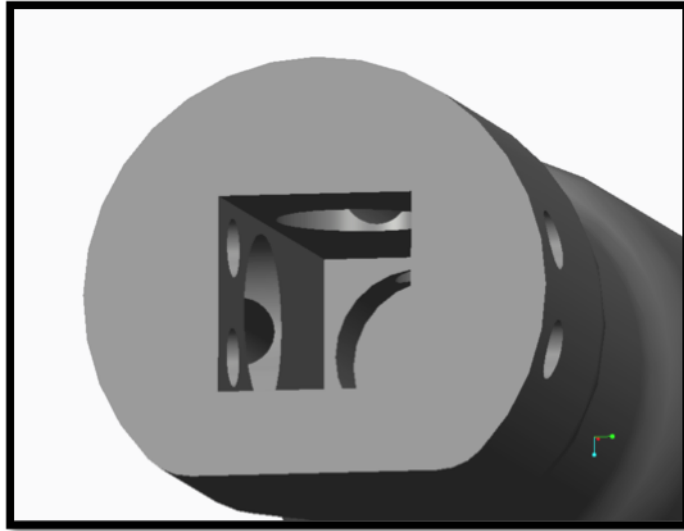


Fig. 2.7. Sensor Placements for the Compression Load Cell Model

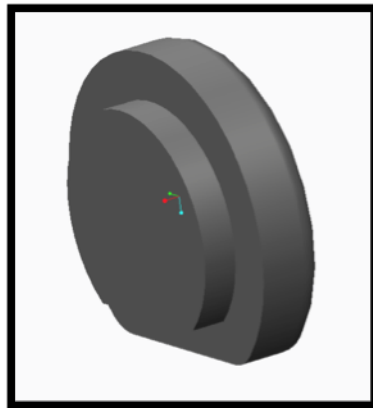
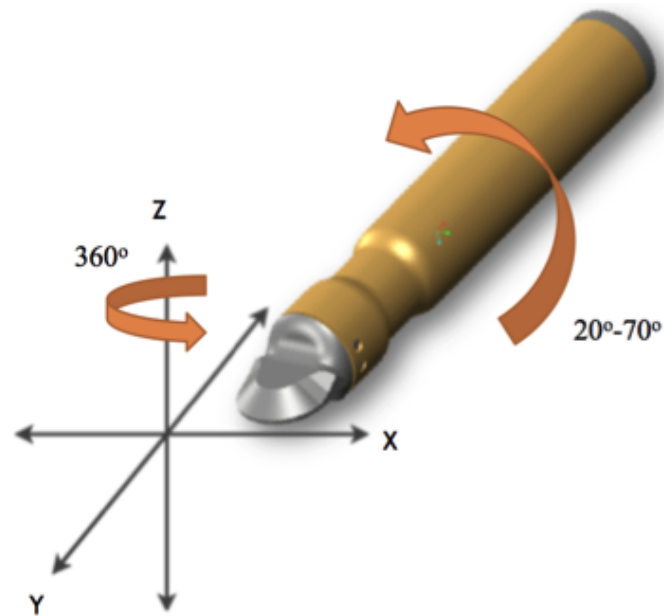


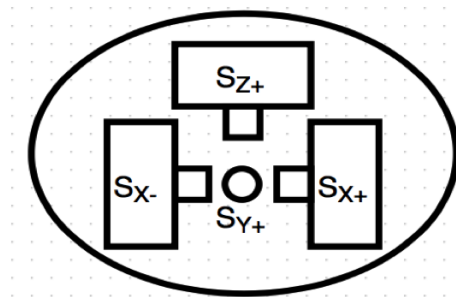
Fig. 2.8. Back Cover of the Compression Load Cells Device

In terms of force measurements, this design used combinations of the compression load cell to measure the three resultant force components in three-dimensional space. The orientation angles of the IASTM device, which had an effect on the force measurements, were considered in the new device design stage. Figure 2.9(a) presents the orientation angles of the IASTM device with respect to its global coordinates. The angle between the tool and skin generally varies between 20 and 70 degrees in a typical treatment; this is based on the X-Y plane, with free rotation about the Z-axis.

As shown in Figure 2.9(b), the compression load cell design consists of four load cells, which is based on the force analysis of the measured forces.



(a) Device Orientation



(b) Sensors Placement

Fig. 2.9. Mechatronic IASTM Device Orientation Angles and Sensors Placement.

According to the orientation constraints, there were three expected movements, each of which produced three different measurements of force. As shown in Figure 2.9(b), the various load cells were positioned around the measurement cavity based on force factorization. First, the S_{z+} and S_{y+} load cells measure force components where the force was applied perpendicularly at the tip of the IASTM device, as shown

in Figure 2.10. Second, when the force is applied with an angle between 0 and 89 degrees, three force components are measured by the S_{z+} , S_{x-} and S_{y+} load cells, as shown in Figure 2.11. Third, when the force is applied with an angle between 91 and 180 degrees, three force components are measured by the S_{z+} , S_{x+} and S_{y+} load cells, as shown in Figure 2.12. As a result, this force analysis confirmed that there was no need for the fifth load cell since there was no force component in the direction of $-Z$; this would lead to reduced cost of the compression load cell device.

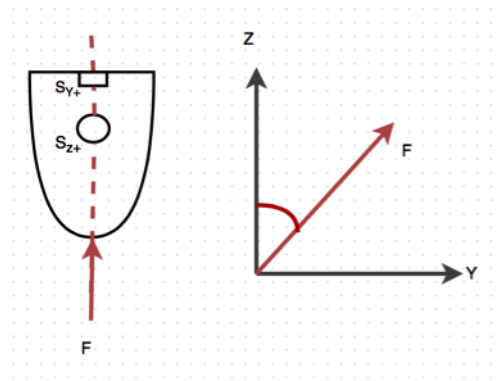


Fig. 2.10. Force Analysis for 90-degree Force Applied to the Tool

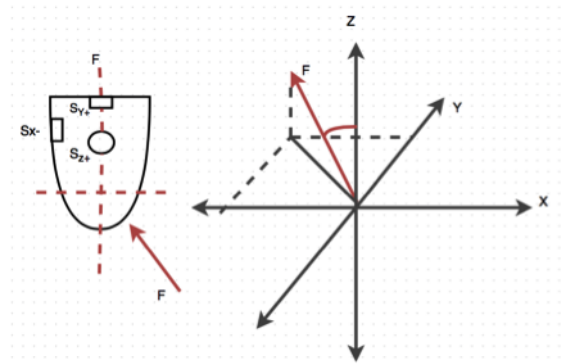


Fig. 2.11. Force Analysis for 0-89 Degrees Force Applied to the Tool

As shown in Figure 2.13, the measurement mechanism of the compression load cell device was based on forces measured by a well-placed four compression load cells and a subsequent transformation to an appropriate coordinate system. Three tiny

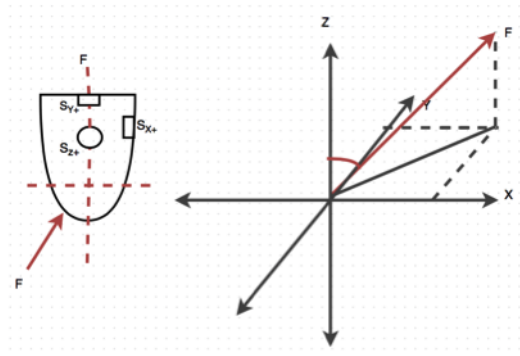


Fig. 2.12. Force Analysis for 91-180 Degrees Force Applied to the Tool

wiring canals were used to connect the wires from the load cell compartment to the microcontroller in the electronics cavity. This design included two keyway pins to lock the tip to the main frame with 3 mm clearance to allow force transmission.

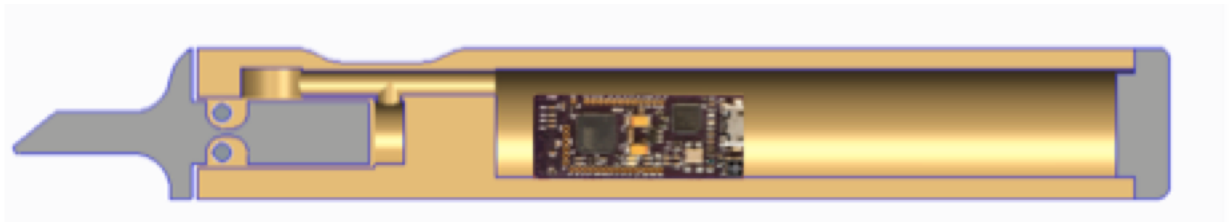


Fig. 2.13. Full Section for the Compression Load Cell Device

2.4 3D Load Cell Based Design

The second design is based on a 3D load cell, which is a single load cell that measures all force components. As shown in Figure 2.14, the 3D load cell design consists of three parts similar to the previous model; however, the main frame is separated into two parts for wiring purposes. These frame parts are assembled using two front internal screws and two back external screws for the back cover, as shown in Figure 2.15(a) and Figure 2.15(b).

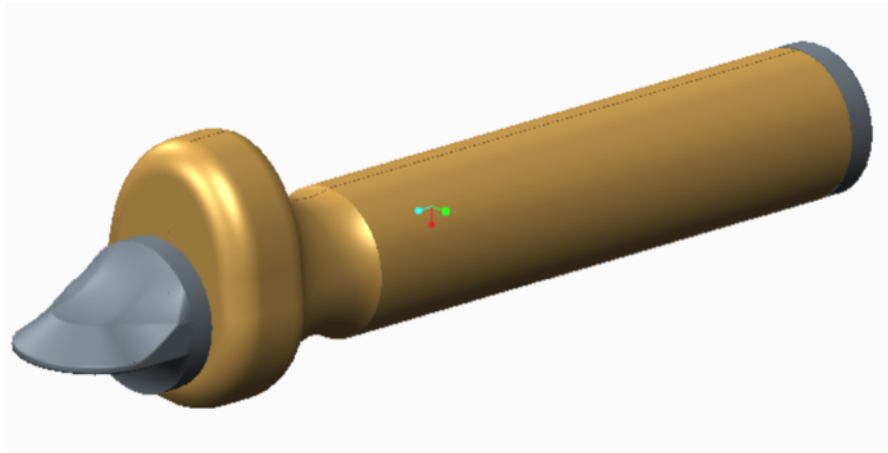
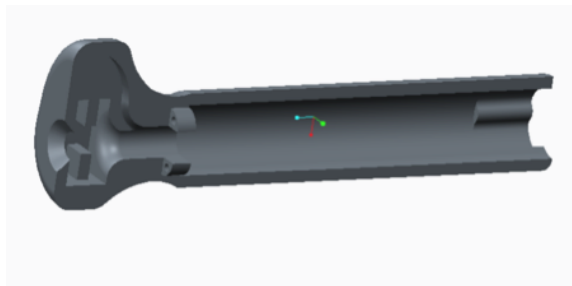
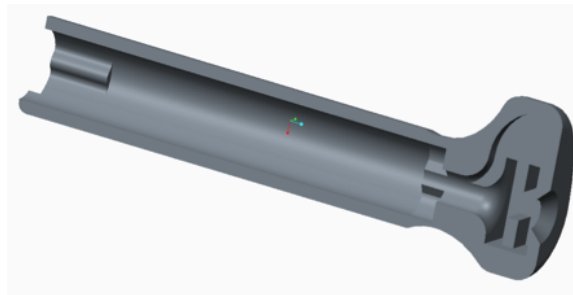


Fig. 2.14. 3D Load Cell Device



(a) Right Side



(b) Left Side

Fig. 2.15. 3D Load Cell Device Frame Parts

Similar to the compression load cell device, the tip was designed to be of the same shape as the IASTM device' tip; as a result, it will have the same precision in targeting soft tissues, as shown in Figure 2.16. A back cavity was designed to fit all

electronics and components needed for the main tasks, as shown in Figure 2.18. The back cover is used to seal and insulate the electronics inside the cavity. It has a small crescent shaped outlet hole for the 3D load cell and microcontroller wires, as shown in Figure 2.17. Part of the cross section of the frame has been narrowed for ergonomic finger placement.

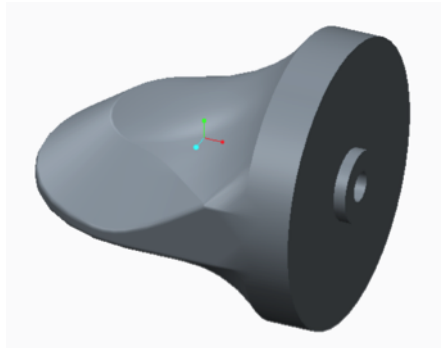


Fig. 2.16. 3D Load Cell Device Tip



Fig. 2.17. 3D Load Cell Device Back Cover

In order to measure the force, the 3D load cell is inserted into the slot, which has been designed on both sides of the frame to fit the dimension of the 3D load cell and its wires, as shown in Figure 2.18. The tip is attached to the 3D load cell using a fully threaded stainless steel screw, and the contact area is the center part of the 3D load cell with a diameter of 6 mm. As a result, the 3D load cell measures all force

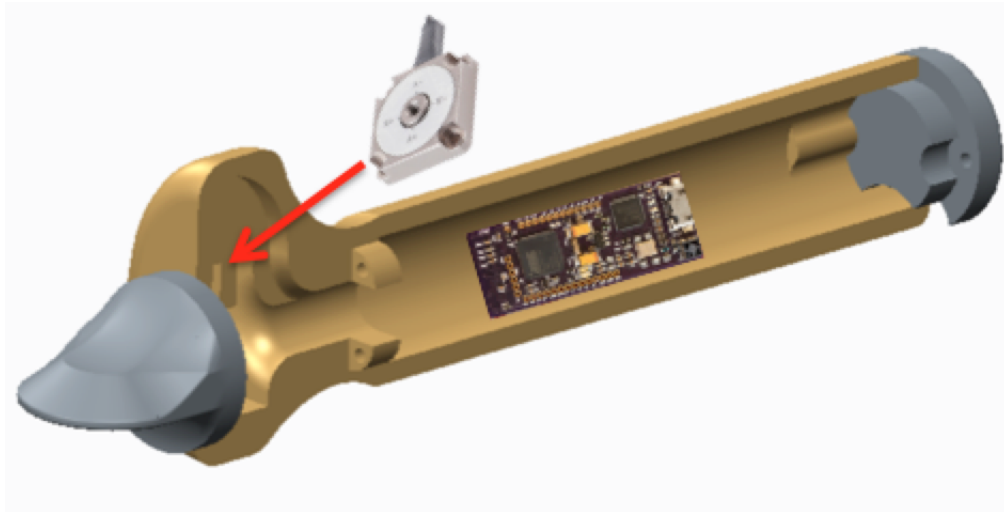


Fig. 2.18. Half Section of the 3D Load Cell Device

components that are being applied to the device's tip. However, the 3D load cell measures the forces applied to its center, and these forces need be transferred to the tool tip/skin interface.

As shown in Figure 2.19, the 3D load cell based device had three different coordinate systems: microprocessor, 3D load cell, and tool tip / skin coordinate. The load cell and microcontroller coordinates were based on their datasheets, while the tool-tip/skin coordinate was assumed to have the following sign convention: device forward (+Y), right (+X), and upward movement (+Z), which was based on the right hand rule.

It was important to transfer the force measurements to the tool-tip/skin interface because the forces at this interface were the main concern for the treatment practice. To perform the force transformation, the microcontroller coordinate was rotated by 90 degrees counterclockwise (CCW) about the X-axis to agree with the 3D load cell coordinates, as shown in Figure 2.20. And this rotation transformation was performed in the orientation measurement code within IMUduino chip [22]. Next, the orientation angles were used to transfer the force measurement to the tool/skin interface since

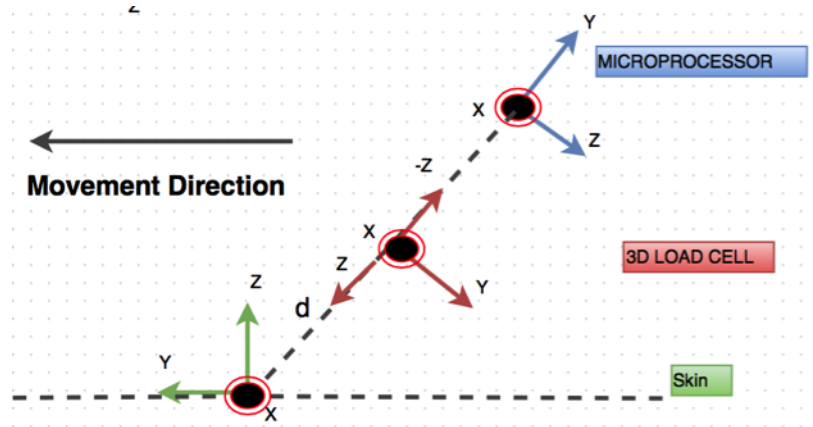


Fig. 2.19. Main Coordinates for the 3D Load Cell Device

the microcontroller and the 3D load cell coordinates agreed with each other, as both coordinates were on the same solid body.

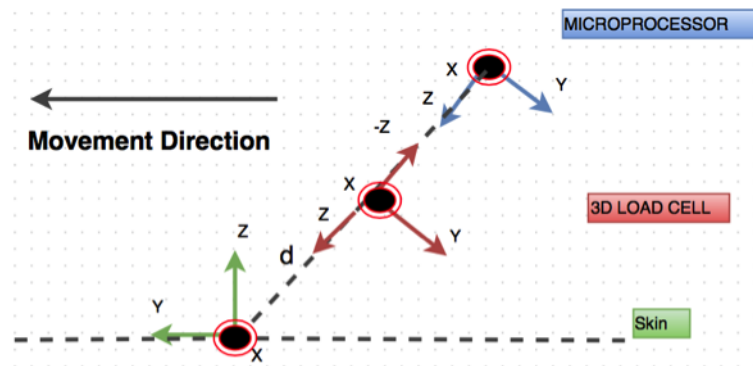


Fig. 2.20. Final Coordinates for the 3D Load Cell Device

Based on Eulers rotation theorem, any arbitrary rotation for a solid object or vector (V) can be represented by a combination of three rotations [24], as shown in Equation 2.1.

$$V' = ROT_x \times ROT_y \times ROT_z \times V \quad (2.1)$$

Where rotations about the X, Y and Z axes are computed using Equations 2.2, 2.3, 2.4. All angles were multiplied by -1 because force components should transfer

back to the origin (horizontal plane) of the 3D load cell coordinate after any rotation in 3D space.

$$ROT_x = \begin{bmatrix} 1 & 0 & 0 & 0 \\ 0 & \cos(-p) & -\sin(-p) & 0 \\ 0 & \sin(-p) & \cos(-p) & 0 \\ 0 & 0 & 0 & 1 \end{bmatrix} \quad (2.2)$$

$$ROT_y = \begin{bmatrix} \cos(-r) & 0 & \sin(-r) & 0 \\ 0 & 1 & 0 & 0 \\ -\sin(-r) & 0 & \cos(-r) & 0 \\ 0 & 0 & 0 & 1 \end{bmatrix} \quad (2.3)$$

$$ROT_z = \begin{bmatrix} \cos(-y) & -\sin(-y) & 0 & 0 \\ \sin(-y) & \cos(-y) & 0 & 0 \\ 0 & 0 & 1 & 0 \\ 0 & 0 & 0 & 1 \end{bmatrix} \quad (2.4)$$

Next, measurements were transferred to the skin with a distance d , which is the distance between the measuring point on the 3D load cell and the tip, and is represented in matrix form, as shown in Equation 2.5.

$$T = \begin{bmatrix} 1 & 0 & 0 & 0 \\ 0 & 1 & 0 & 0 \\ 0 & 0 & 1 & d \\ 0 & 0 & 0 & 1 \end{bmatrix} \quad (2.5)$$

Then, a counterclockwise (CCW) rotation about the X-axis was necessary to transfer the measurements to the proposed practice direction, as shown in Equation 2.6.

$$ROT_{x - skin} = \begin{bmatrix} 1 & 0 & 0 & 0 \\ 0 & \cos(90) & -\sin(90) & 0 \\ 0 & \sin(90) & \cos(90) & 0 \\ 0 & 0 & 0 & 1 \end{bmatrix} \quad (2.6)$$

Finally, to get the transformed force measurement on the skin surface, the force vector was multiplied by the distance matrix, Eulers rotation matrix and the assumed practice direction matrix, respectively, as shown in Equation 2.7. Where Equation 2.6 was used to transfer the force measurement to the skin coordinate.

$$F' = ROT_{x - skin} \times ROT_x \times ROT_y \times ROT_z \times T \times F \quad (2.7)$$

Equation 2.7 was computed using Matlab code, to represent each force component in a separate formula, as shown in Equations 2.8, 2.9, 2.10.

$$Fx' = d \times \sin(-r) + Fz \times \sin(-r) + Fx \times \cos(-r) \times \cos(-y) Fy \times \cos(-r) \times \sin(-y) \quad (2.8)$$

$$\begin{aligned} Fy' = & -Fx \times (\sin(-p) \times \sin(-y) - \cos(-p) \times \cos(-y) \times \sin(-r)) \\ & - Fy \times (\cos(-y) \times \sin(-p) + \cos(-p) \times \sin(-r) \times \sin(-y)) \\ & - Fz \times \cos(-p) \times \cos(-r) - d \times \cos(-p) \times \cos(-r) \end{aligned} \quad (2.9)$$

$$\begin{aligned} Fz' = & Fx \times (\cos(-p) \times \sin(-y) + \cos(-y) \times \sin(-p) \times \sin(-r)) \\ & + Fy \times (\cos(-p) \times \cos(-y) - \sin(-p) \times \sin(-r) \times \sin(-y)) \\ & - Fz \times \cos(-r) \times \sin(-p) - d \times \cos(-r) \times \sin(-p) \end{aligned} \quad (2.10)$$

To verify and examine these formulas, different orientation angles were proposed under measured 100 N compression force and substituted in the overall force transformation matrix, as shown in Table 2.1. The data obtained were broadly consistent

with different orientation angle sets and the shifting distance of the 3D load cell from the skin surface.

Table 2.1
Resultant Forces on Skin with Different Orientation Angles Under
100N Compression Force

Only Rotation	Force(N)		Combination (Rotation and Translation)	Force(N)
Yaw=0 Pitch=0 Roll=0	Fx= 0 N Fy=100 N Fz=0 N		Yaw=0 Pitch=45 Roll=0 Trans-z=2	0 69.2965 -69.2965
Yaw=0 Pitch=45 Roll=0	Fx= 0 N Fy=70.7107 N Fz=-70.7107 N		Yaw=0 Pitch=45 Roll=0 Trans-z=4	0 67.8823 -67.8823
Yaw=0 Pitch=0 Roll=45	Fx= 70.7107 N Fy=70.7107 N Fz=0 N		Yaw=0 Pitch=45 Roll=0 Trans-z=6	0 66.4680 -66.4680
Yaw=45 Pitch=0 Roll=0	Fx= 0 N Fy=100 N Fz=0 N		Yaw=0 Pitch=0 Roll=45 Trans-z=6	66.4680 66.4680 0

An external amplifier (DSA-03A) is used to filter and amplify the output signal of the 3D load cell, which is then introduced to the Labview software using the data acquisition card (DAQ), as shown in Figure 2.21. In addition, the microcontroller (IMUduino), that measures the orientation angles, is connected directly to the computer (PC) using a USB programming cable.

The 3D load cell sensor measures strains in the 3D space, (Appendix A). The force components are obtained by multiplying strain readings in 3D space by the

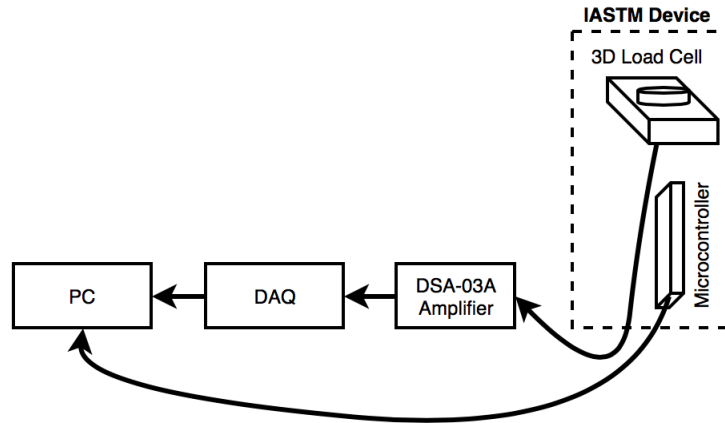


Fig. 2.21. 3D Load Cell Device System Configuration

calibration matrix, as shown in Equation 2.11. However, the sensor output is in volts, where one volt is equal to 400 micro strains.

$$\begin{pmatrix} FHx \\ FHy \\ FHx \end{pmatrix} = \begin{pmatrix} 0.23017 & -0.00226 & 0.00360 \\ 0.01763 & 0.22724 & -0.00208 \\ -0.00267 & 0.00122 & 0.26504 \end{pmatrix} \begin{pmatrix} \epsilon x \\ \epsilon y \\ \epsilon z \end{pmatrix}$$

FHx, FHy, FHx : Load value (N) after correction
 $\epsilon x, \epsilon y, \epsilon z$: Strain Output ($\times 10^{-6}$ Strain)

(2.11)

2.4.1 Labview Model Building for 3D Load Cell Device

Force Measurement Model

Force measurement was filtered and amplified using the external amplifier (DSA-03A), which provided the force variation in terms of voltage within ± 5 Volt for the three axes using three cables. These cables were connected to the DAQ device, and a Labview model was created to get the final force measurement for each axis, as shown in Figure 2.22. The force measurement model consisted of three phases, which were signal enquiring, gains multiplication, and calibration and transformation. DAQ

assistant was used in a while loop to extract the force signal from the DAQ and send it to the labview model continually. The DAQ assistant displayed the input signals, which were adjusted to zero using the external amplifiers trimmers. Then two different gains were multiplied by the input signals. The gains for the X and Y axes were 200 each, and 400 was the gain for the Z axis according to the manufacturer. Then, force signals were stored in matrix form and multiplied by the calibration matrix 2.11. The resultant force measurement matrix was translated along the Z-axis and rotated around the X- axis 90 degrees using Eulers rotation matrix with a rotation order of X-Y-Z, respectively.

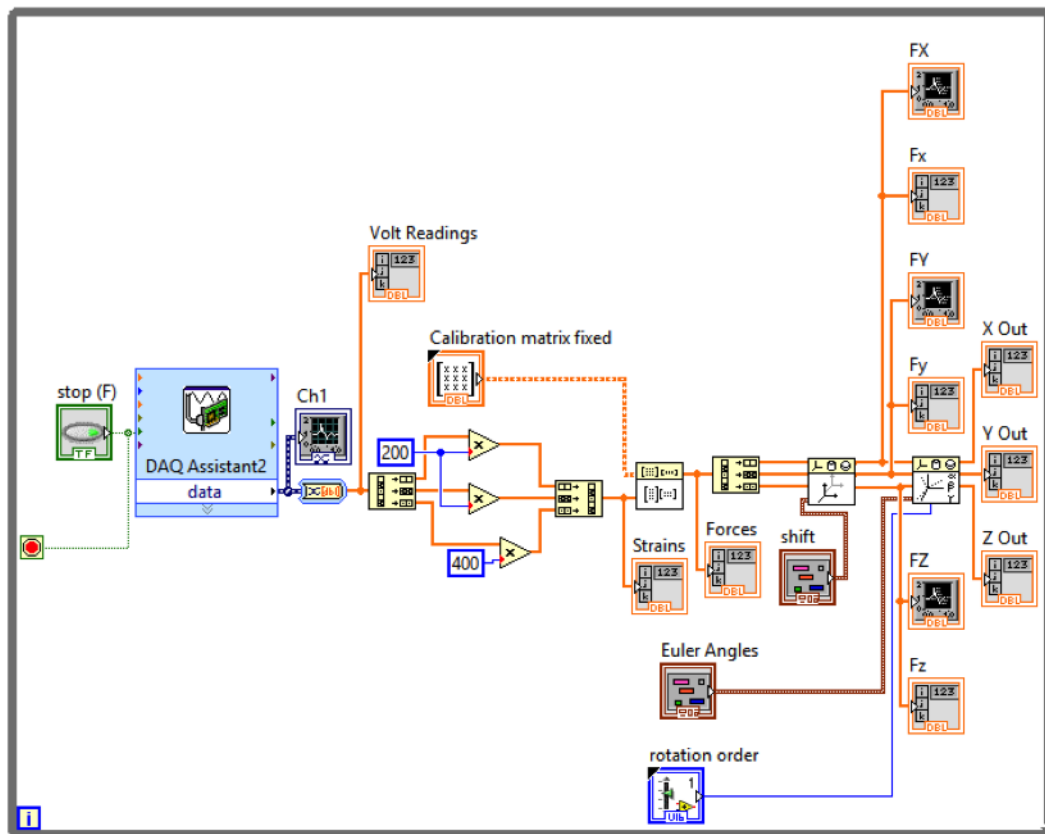


Fig. 2.22. Force Measurement Labview Model for the 3D Load Cell Design

Orientation Measurement Model

The IASTM orientation angles with respect to horizontal treatment surface were measured using the microcontroller (IMUduino), which used the open source modified code Free IMU-Yaw-Pitch-Roll (Appendix B). The arduino code sends the measured angles to Labview using a serial USB cable in a specific modified form (x -YAW- y -ROLL- z -PITCH). In Labview, a model was developed to interpret the previous angle measurement string, which was sent to Labview by the IMUduino, using NI-Visa block to communicate with a serial port, as shown in Figure 2.23. The orientation measurement model extracted the angles based on the placements of the three characters x, y and z.

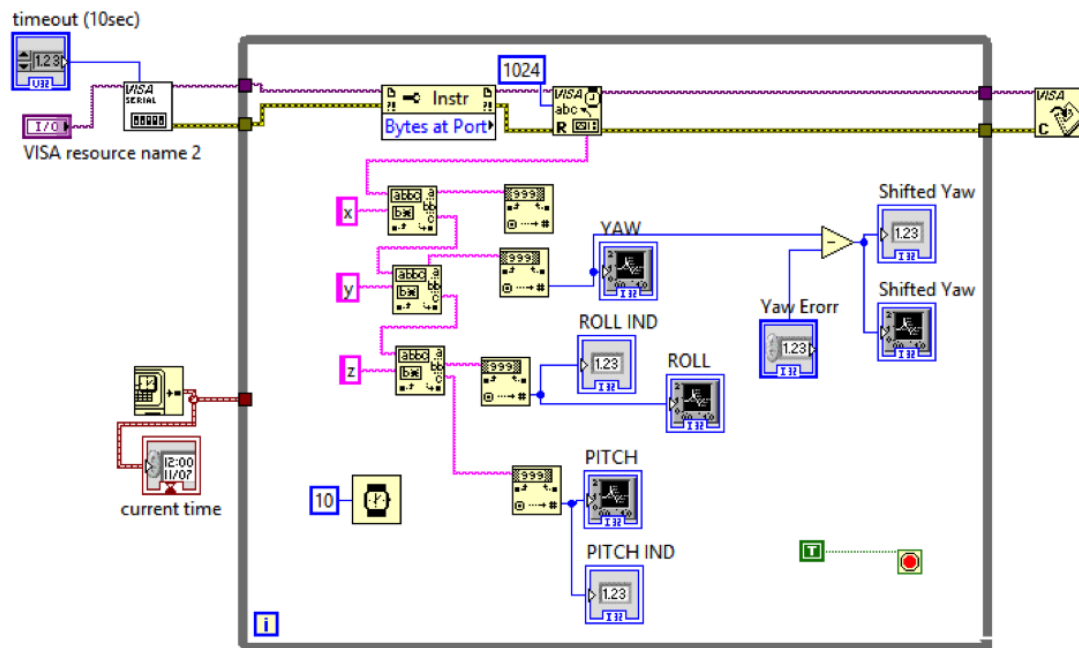


Fig. 2.23. Orientation Measurement Labview Model for the 3D Load Cell Design

The IASTM Measurement Model

As shown in Figure 2.24, the angle and orientation measurement models were assembled in one final model, to use the momentary angles in the force transformation. In this thesis, only pitch angle was considered in the force transformation because it was cortical in the IASTM practice; roll and yaw assumed to be zero. Pitch angle was converted to radian since Euler rotation block uses radian angles in Labview. Besides angle and force measurements, the IASTM device provided postprocessing data, which included critical parameters in the treatment. These parameters were: average angles, average forces within 200 samples, maximum and minimum measured force for each axis, resultant force using Equation 2.12, average peak resultant force, stroke number and stroke frequency per minute.

$$\text{Resultant Force} = \sqrt{Fx^2 + Fy^2 + Fz^2} \quad (2.12)$$

The stroke counter used the peak detection for the measured force of Z-axis function in Labview, where the threshold and signal width were set to be 5 N and 3 sec, respectively. All measurements could be exported in Excel format file for practice analysis. As shown in Figure 2.25, a user-friendly front panel was created to present all necessary data for the physician during the IASTM practice.

2.5 IASTM Tool Fabrication Using 3D Printing Technology

The prototypes of the proposed designs were fabricated or printed using 3D printing technology, which is a relatively new technology in additive manufacturing. The 3D printed prototypes are shown in Figures 2.26 and 2.27. 3D printing is the process of transforming a CAD design into a physical model, which is printed layer by layer until the model is completed, using Fused Deposition Modeling (FDM). All hung parts and cavities are filled by the printer with removable supporting materials, which can be removed using hand tools or specific solutions. All CAD files were transformed into STL (STereoLithography) format using Creo Parametric 2.0. The 3D printer (uPrint

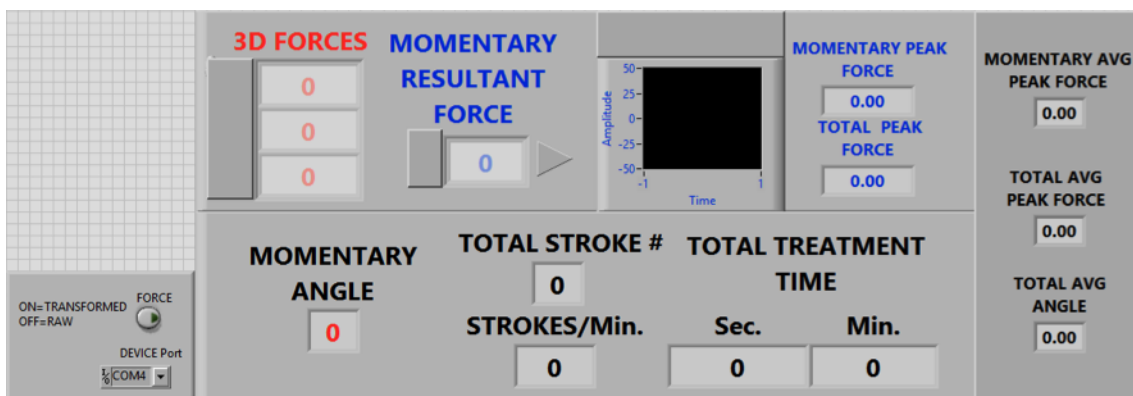


Fig. 2.25. The IASTM Device Front Panel



Fig. 2.26. 3D Printed Model of Compression Load Cell Device



Fig. 2.27. 3D Printed Model of 3D Load Cell Device

3. FINITE ELEMENT ANALYSIS OF THE PROPOSED DESIGNS

3.1 Modeling Initialization

Finite Element Analysis (FEA) is a numerical method used to analyze and simulate various mechanical systems, such as thermal, structural, electromagnetic and fluid dynamics systems. In this research, the proposed designs of the mechatronic IASTM tool are modeled, analyzed, and simulated as a mechanical structure with simplifying assumptions on the elastic behavior of the skin under a certain amount of force. A finite element model of a human arm is simulated to show the relationship between the applied forces, stress and strain on skin, and force measurements.

3.1.1 Skin and Tissue Modeling

For the purposes of this study, the human tissues and layers were modeled in Creo Parametric 2.0 as a $100mm^3$ box with four curved edges to be similar to an arm, as shown in Figure 3.1. A cylindrical hollow of 30 mm diameter was designed for bone placement. The skin model was imported to ANSYS Workbench R15.0 to perform the simulation.

Human tissue is a very complex structure in the human body which has four main layers: skin, subcutaneous adipose tissue, muscle, and bone, each of which has different mechanical properties. Agache al. [25] has presented these mechanical properties and Youngs modulus of human skin in vivo, and showed that Youngs modulus varies between 0.42 MPa and 0.85 MPa. According to the Physics Hyper textbook [26], skin density was shown to be about $1050Kg m^{-3}$. In a study of characterization of the mechanical properties of skin by inverse analysis combined with the indentation

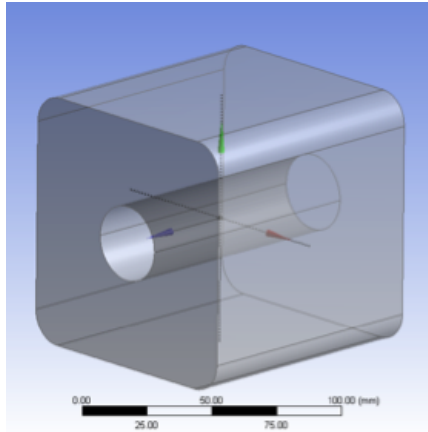


Fig. 3.1. Human Arm Model in ANSYS

test [27], Poisson's Ratio was estimated to be 0.48 using the indentation test. The ultimate tensile strength (UTS) has been determined to be between 5.7 and 12.6 MPa [28] and has been selected to be the UTS of all tissue layers, as shown in Table 3.1. The friction coefficient between skin and stainless steel found to be to be 1 [29].

Table 3.1
Mechanical Properties of Human Skin

Parameter	Value
Element Type	3D Solid Quadrilateral Isotropic
Density	1050 kg/m ³
Young's Modulus	0.82 MPa
Poisson's Ratio	0.48
UTS	12.6 MPa

As shown in Figure 3.2, a finite element mesh was generated for the human skin model, which holds the skins mechanical properties, in order to compute the resultant stress-strain at each node on the skin. The more mesh the model had, the more accurate the result became. However, increasing the mesh size resulted in increasing the solution time. As a result, a mesh refinement was performed on the skin surface, since the purpose of this study was to show skin reaction to the applied forces.

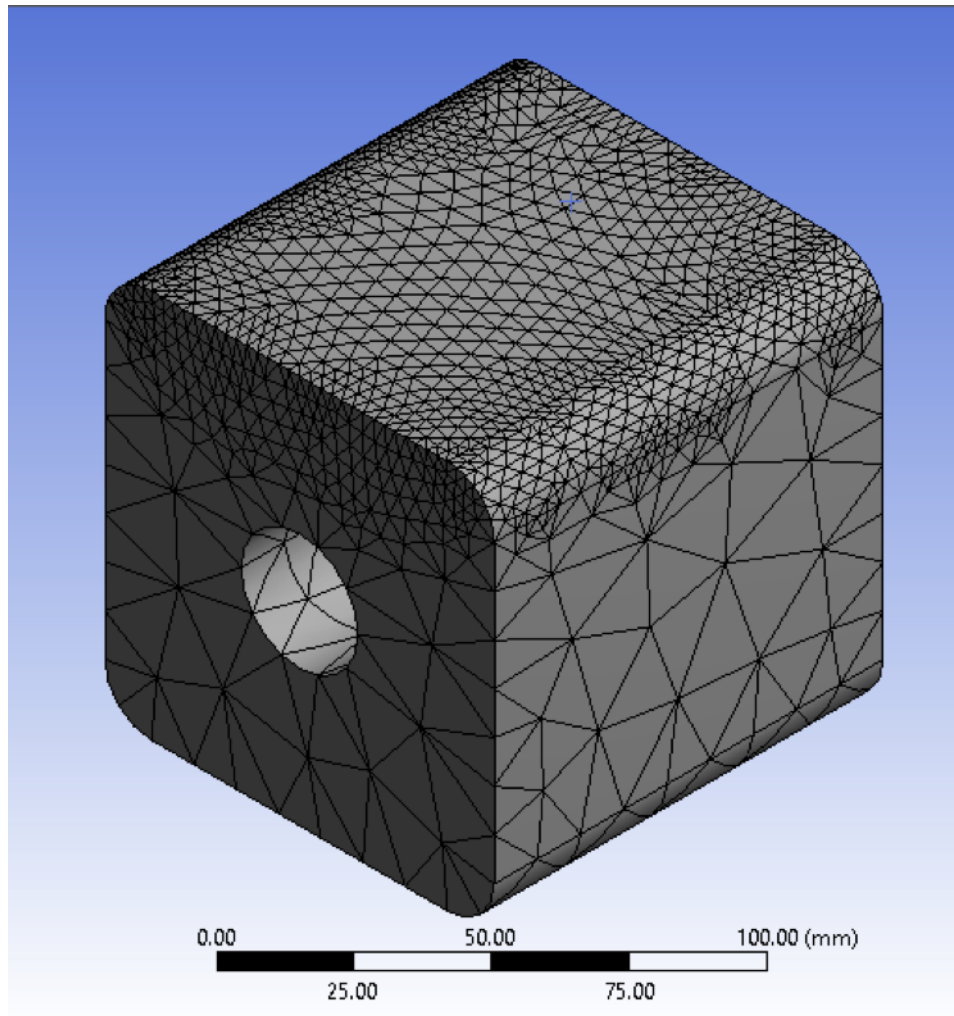


Fig. 3.2. Skin Meshing

3.1.2 IASTM Modeling

The device, which was based on four compression load cells, was imported to ANSYS workbench R15.0 to perform the simulation, as shown in Figure 3.3. As shown in table 3.2, stainless steel was selected to be the material for both the tip and tail of the IASTM device. Different assumptions were utilized to simplify the analysis; the back cover was welded to the device tail. In addition, the four compression load cells were embedded into the devices front end of the tail, where the devices front end and the four load cells were part of the tail made of stainless steel, as shown in Figure 3.4.

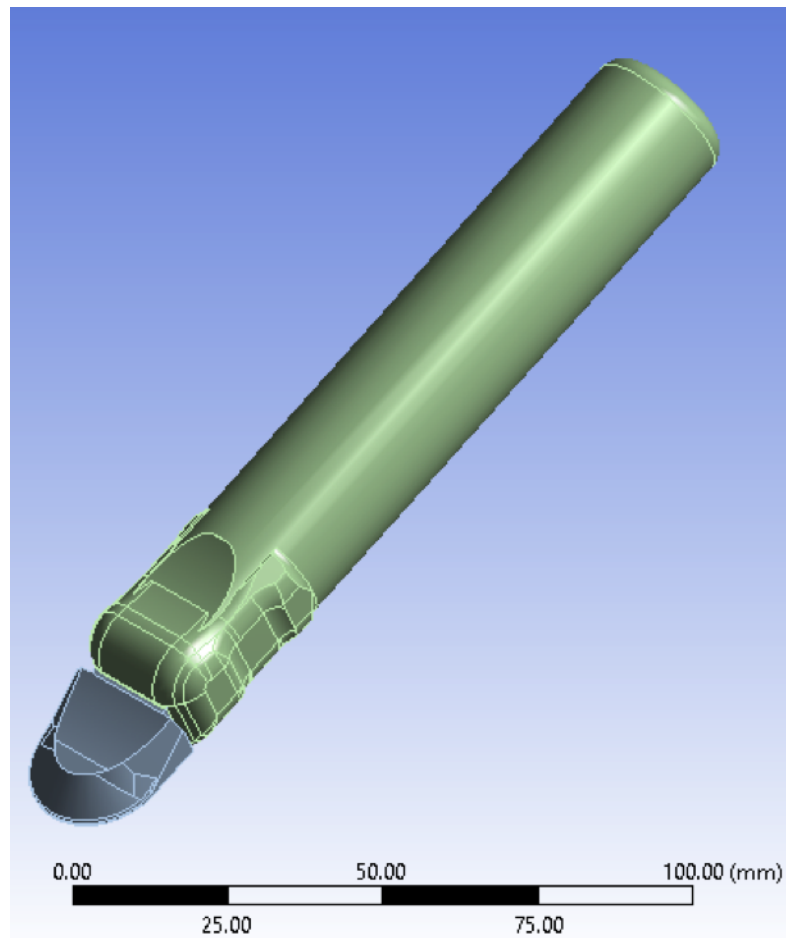


Fig. 3.3. Compression IASTM Load Cell Device in ANSYS

Table 3.2
Mechanical Properties of the Compression IASTM Load Cell Device

Parameter	Value
Density	7750 kg/m ³
Young's Modulus	1.93x10 ⁵ MPa
Poisson's Ratio	0.31
UTS	586 MPa

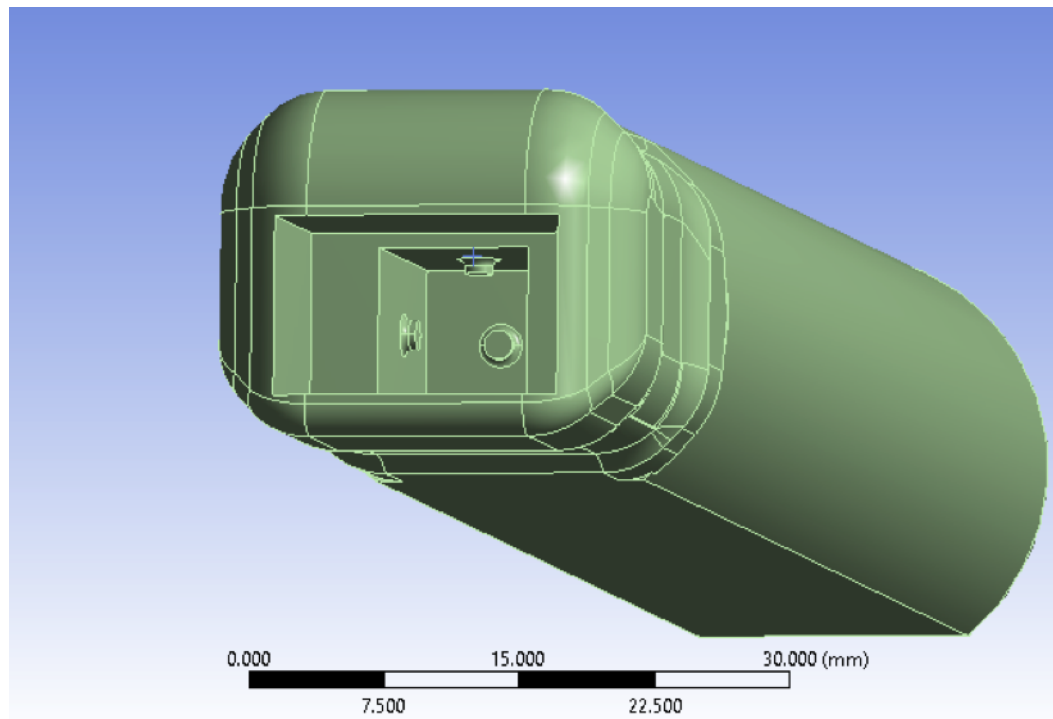


Fig. 3.4. Compression Load Cell Embedded into the Device Tail

Meshing was generated for both the tip and tail models, as shown in Figure 3.5. Since the purpose of this analysis was to evaluate stress and the applied force on the

skin with respect to force measurement, the load cells tips mesh was refined to obtain accurate force analysis, as shown in Figure 3.6.

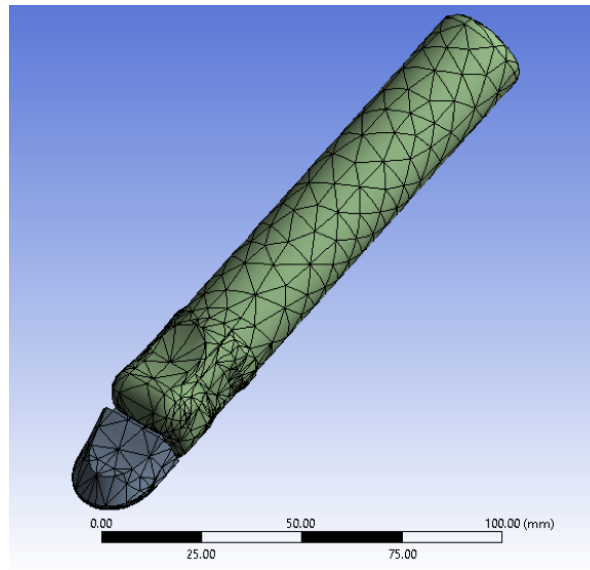


Fig. 3.5. Meshed Load Cell Device

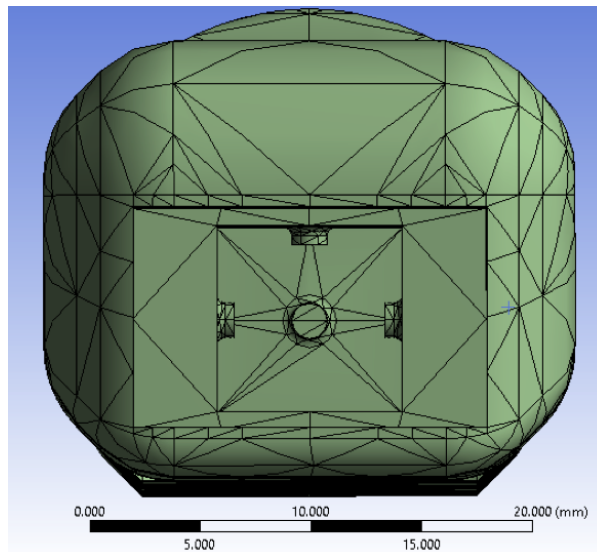


Fig. 3.6. Meshed Load Cell Tail

3.1.3 Simulation Scenarios Setup

After the compression load cell device and the skin model were imported to the ANSYS Workbench, connections and the static structural setting had to be defined to conduct the simulation. The finite element analysis of the 1D compression load cell device had two scenarios, which were based on the mechanical connection between the devices tip and skin surface. These scenarios were the frictional and bonded connections.

Frictional Contact Scenario

The device's tip was linked to the tail with small tolerance, so force could be transferred from the device's tip to the four compression load cells when force was applied to the patients skin. As a result, the connection between the tip and the tail was assumed to be a bonded connection, where nine faces on both parts were defined to be the connection areas, as shown in Figures 3.7 and 3.8.

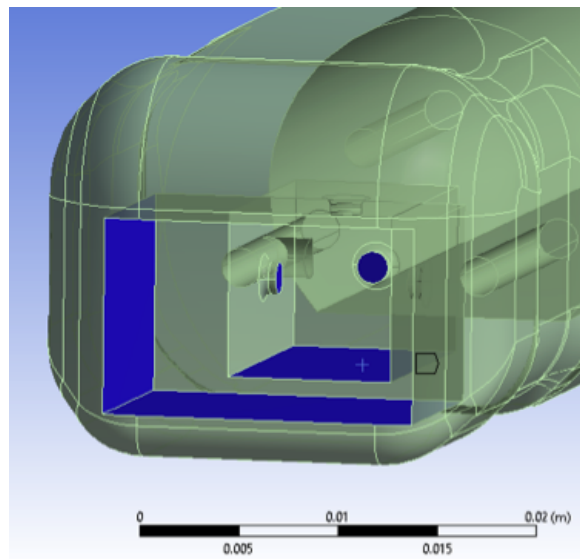


Fig. 3.7. Device Tail Bonded Connection

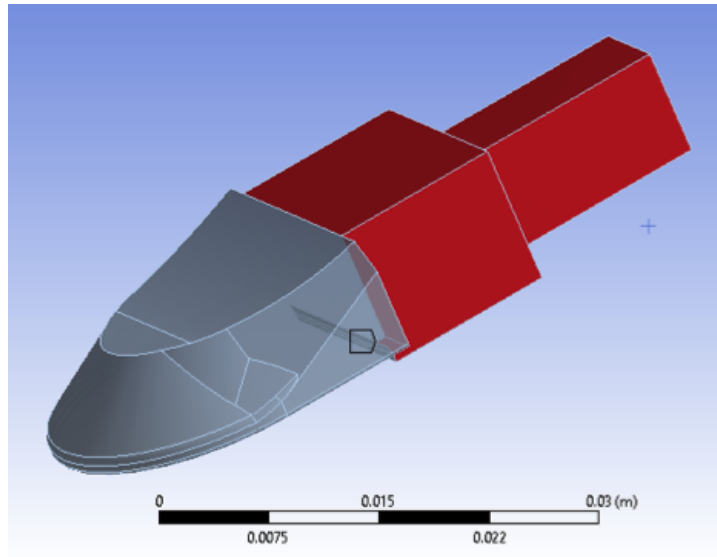


Fig. 3.8. Device Tip Bonded Connection

In the IASTM treatment, tools interact with human skin in different areas, and most of these tools, which are used in physical therapy clinics, are made of stainless steel. The contact between the polished stainless steel and skin is a frictional contact, even when gel is used to minimize the friction. As a result, the connection between skin and the device tip was determined to be a frictional connection with friction coefficient $\mu = 1$ [29]. The frictional coefficient plays an important role in defining the relationship between two materials and normal force, and the frictional coefficient between skin and stainless steel has been found to be one [29]. The contact areas were defined as four faces on the device tip and the upper area of the arm model, as shown in Figures 3.9 and 3.10. The Augmented Lagrange formulation was used to define the contact area and prevent interaction between two bodies using Equation 3.1, where λ made the solution less sensitive to contact stiffness [30].

$$F_{normal} = k_{normal} \times a_{penetration} + \lambda \quad (3.1)$$

After the connections were defined, the contact initial information could be generated and investigated using contact tools, as shown in Table 3.3. The table shows all

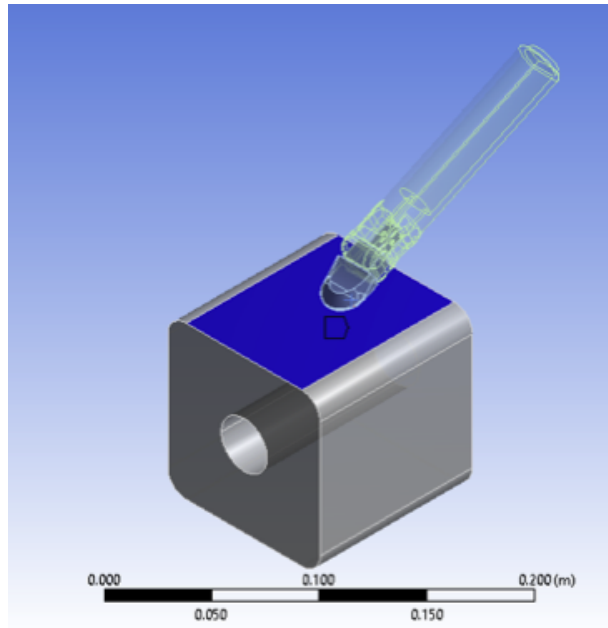


Fig. 3.9. Skin Frictional Contact Area

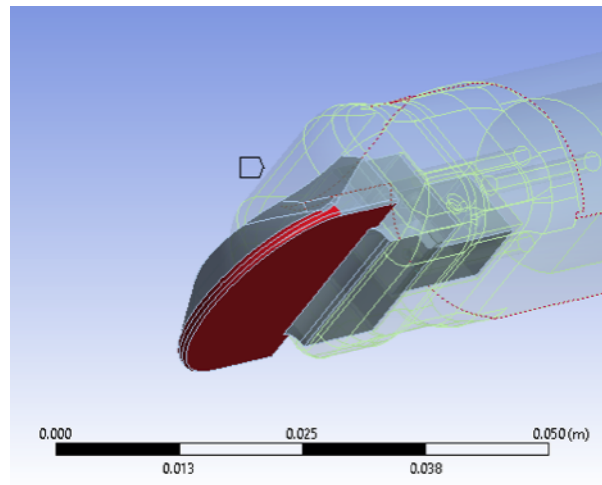


Fig. 3.10. Device Tip Frictional Contact Areas

connections, geometric gaps, and penetration, and the resulting pinballs radii, which provide an efficient contact calculation by differentiating the far and near contact regions while identifying the expected contact elements [30].

Table 3.3
Initial Information for IASTM Device Simulation Using Contacts Areas

Name	Contact Side	Type	Status	Number Contacting	Penetration (mm)	Gap (mm)	Geometric Penetration (mm)	Geometric Gap (mm)	Resulting Pinball (mm)	Real Constant
Frictional - HEAD-FC08 To SKINAN DBONE	Contact	Frictional	Closed	20	0.47947	0	0.47947	N/A	2.8661	4
Frictional - HEAD-FC08 To SKINAN DBONE	Target	Frictional	Closed	3	0.29081	0	0.29081	N/A	7.6143	5
Bonded - HEAD-FC08 To TAIL-FC08	Contact	Bonded	Closed	62	1.53E-14	0	6.58E-09	7.52E-09	0.71892	6
Bonded - HEAD-FC08 To TAIL-FC08	Target	Bonded	Closed	103	1.53E-14	0	6.84E-09	7.81E-09	0.42188	7

The static structural and boundary conditions were defined after meshing was performed and the contact information was generated. The analysis time was set for 6.3 seconds, and the number of steps was 12. For the nonlinear controls of the static structure, the unsymmetrical Newton Raphson option was selected to help with convergence of the solution. In the real practice of IASTM, the device is moved with certain acceleration on a skin surface. Therefore, the device acceleration was assumed to be $0.5\text{mm}/s^2$ in a direction parallel to the skin surface (Z axis), as shown in Figure 3.11.

The displacement constraint was set as follows: the bottom surface of the device was selected to apply the displacement condition, as shown in Figure 3.12. The device was set free to move against the skin, which was represented by the Z direction in the device coordinate system. Similarly, the device was set to move across and parallel to

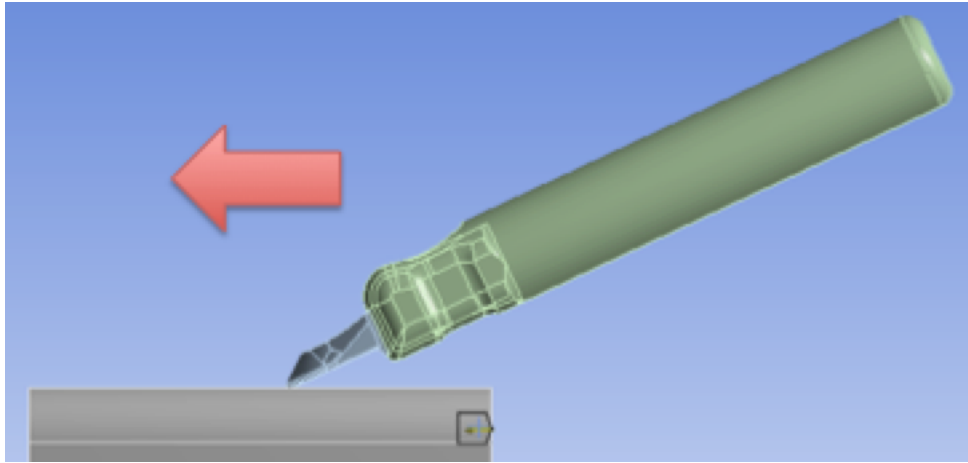


Fig. 3.11. Direction of Devices Acceleration

the skin with an acceleration of $0.5\text{mm}/\text{s}^2$. But the device was not allowed to have sideways movements, which means it couldn't move in X direction.

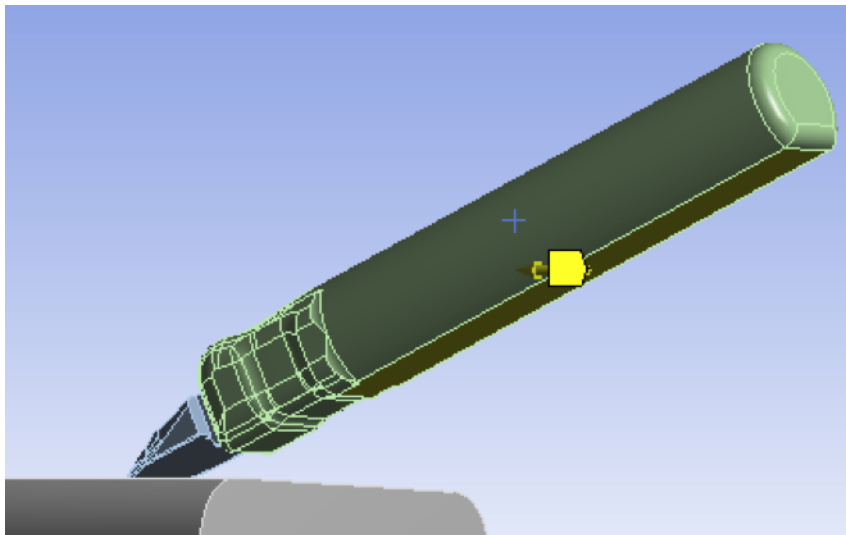


Fig. 3.12. Device Displacement Constraint Areas

IASTM has different treatment positions and methodologies, where force is applied to different parts of the device. For the new IASTM device, the force can be applied to device either on the tool neck or on the back cover, as shown in Figures 3.13 and 3.14. In both cases, the same pressure amount will be delivered to the skin. In this

FEA, a compression force was chosen to be applied gradually to an area of 207.14mm^2 on the back cover to test the IASTM under different pressures/forces and to assist with the force convergence, as shown in Table 3.4.



Fig. 3.13. Applied Force to IASTM Device on the Tool Neck



Fig. 3.14. Applied Force to IASTM Device on the Back Cover

Table 3.4
Hand Pressure on the Back of Device in FEA (Frictional Connection)

Steps	Time [s]	Pressure [MPa]
1	0	0
	1	0.1
2	2	
3	3	0.2
4	4	
5	5	
6	6	0.25
7	7	

Bonded Contact Scenario

Similar to the frictional scenario, the device tip was linked to the tail with small tolerance. The connection between the tip and the tail was assumed to be a bonded connection, where nine faces on both parts were defined to be the connection areas, as shown in the previous section, in Figures 3.7 and 3.8. In the bonded scenario, in order to investigate the impact of the IASTM device on skin and its force measurement, the contact between the polished stainless steel and skin was considered a bonded connection, which means both objects were glued together and not allowed to separate. The contact areas were defined as four faces on the device tip and the upper area of the arm model, as shown in the previous section, in Figures 3.9 and

3.10. The contact initial information was generated and investigated using contact tools, as shown in Table 3.5.

Table 3.5
Initial Information for AISTM Device Simulation Using Contacts Areas

Name	Contact Side	Type	Status	Number Contacting	Penetration (mm)	Gap (mm)	Geometric Penetration (mm)	Geometric Gap (mm)	Resulting Pinball (mm)	Real Constant
Bonded - HEAD-FC08 To SKINANDBONE	Contact	Bonded	Closed	22	0	0	0.344 97	0.351 68	0.358 27	4
Bonded - HEAD-FC08 To SKINANDBONE	Target	Bonded	Inactive	N/A	N/A	N/A	N/A	N/A	N/A	5
Bonded - HEAD-FC08 To TAIL-FC08	Contact	Bonded	Closed	62	1.57E -14	0	6.58E -09	7.52E -09	0.718 92	6
Bonded - HEAD-FC08 To TAIL-FC08	Target	Bonded	Closed	103	3.14E -14	0	6.84E -09	7.81E -09	0.421 88	7

The static structural and boundary conditions were defined after meshing was performed and the contact information was generated. The analysis time was set for 12 seconds, and the number of steps was 12. For the nonlinear controls of the static structure, the program controlled Newton Raphson option was selected to help with convergence of the solution.

The displacement constraint was set as follows: the bottom surface of the device was selected to apply the displacement condition, as shown in Figure 3.15. The device

was set free to move against the skin, which was represented by the Z direction in the device coordinate system. But the device was not allowed to have sideways movements (X-axis) or vertical movements (Y-axis). The force was applied gradually to an area of $207.14mm^2$ on the back cover to test the IASTM under different pressures /forces and to assist with the force convergence, as shown in Table 3.6.

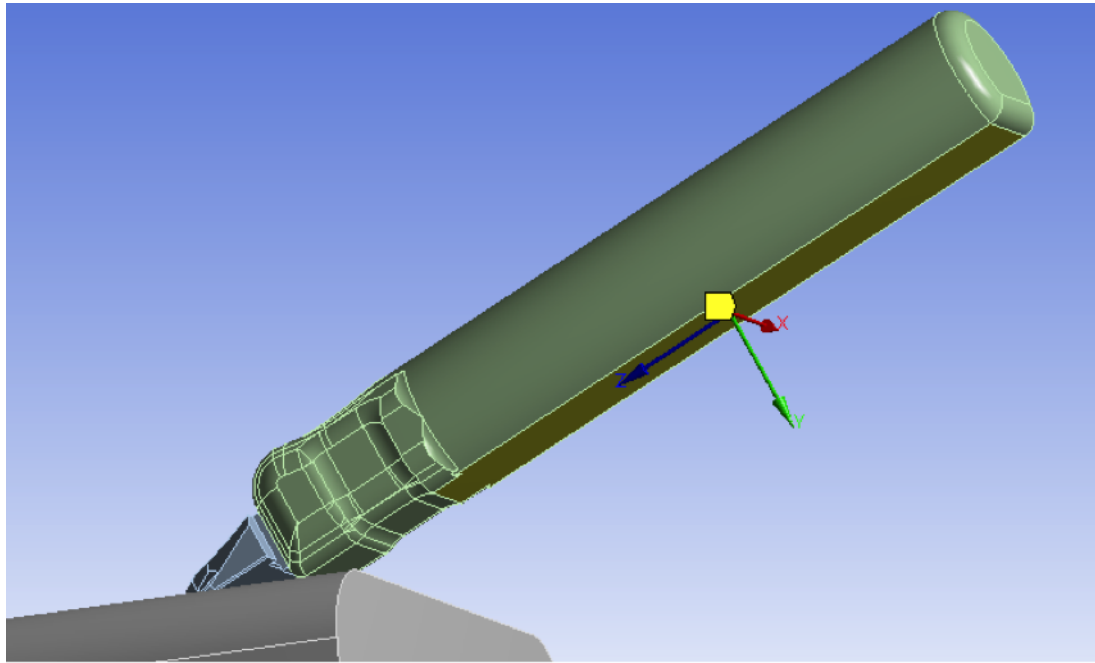


Fig. 3.15. Device Displacement Constraint Areas

3.2 Analysis Results and Discussion

3.2.1 Frictional Scenario

After all the IASTM device simulation parameters were defined, the simulation was successfully solved to compute the desired stresses and strains on different components, which resulted from the applied hand force by a therapist, using ANSYS Workbench R15.0. As shown in Figure 3.16, the force convergence chart shows which sub-step or load step converged at each iteration, to check the simulation validity.

Table 3.6
Hand Pressure on the Back of Device in FEA (Bonded Connection)

Steps	Time [s]	Force[N]
1	0	10
	1	15
2	2	30
3	3	45
4	4	60
5	5	70
6	6	75
7	7	80
8	8	85
9	9	90
10	10	95
11	11	110
12	12	120

The following subsections explore the relationship between stress and deformation on the skin, which resulted from hand pressure measured by the load cell's tips.

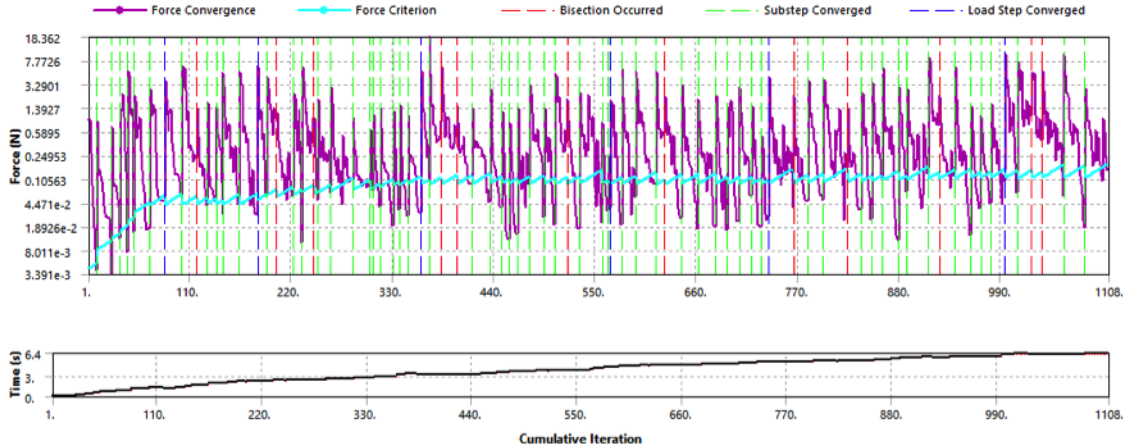


Fig. 3.16. Force Convergence Chart (Frictional Connection)

Simulated Skin Results

Von Mises Stress (Equivalent Stress) and Maximum Principal Stress were generated to determine the relationship between the hand pressure and the stresses on the skin. These methods are used widely to detect the failure criteria of different material under certain forces. As shown in Figure 3.17, the relationship between the Von Mises Stress (Equivalent Stress) and hand pressure was produced using the ANSYS. Its clear that when the hand pressure increased, the maximum and minimum Equivalent Stress also increased. In terms of maximum Equivalent Stress, the maximum value was recorded after the hand pressure was increased to 0.20 MPa, at 2.49 seconds, as shown in Figure 3.18. The minimum value was recorded at the beginning of the practice, at 0.10 seconds, when the device just touched the skin with a pressure of 0.0281 MPa.

The relationship between the minimum and maximum readings for the Maximum Principal Stress was generated, as shown in Figure 3.19. The maximum value of the Maximum Principal Stress represents the tension stress on skin, which increases when the hand pressure increases. In addition, the compression stress (minimum values)

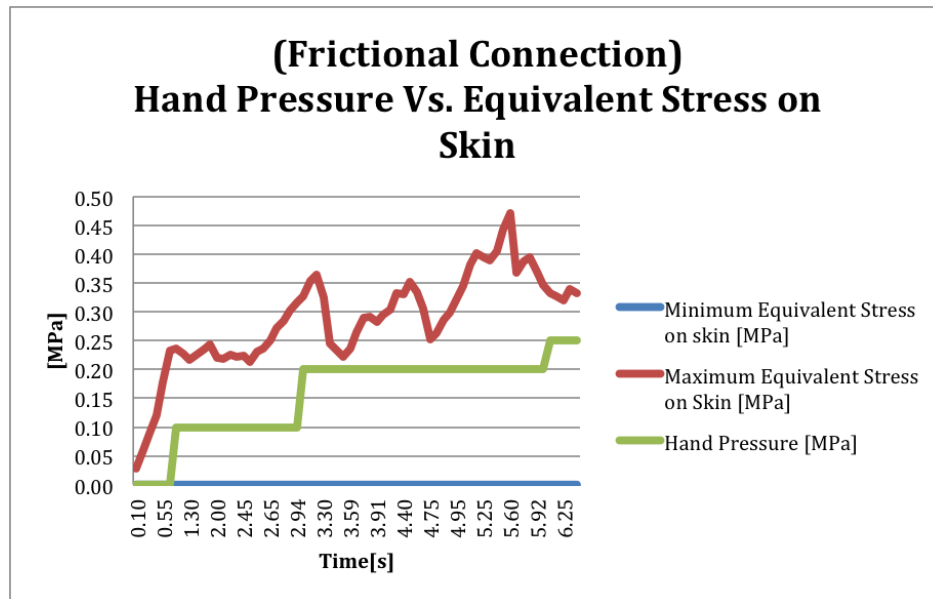


Fig. 3.17. Hand Pressure vs. Equivalent Stress on Skin (Frictional Connection)

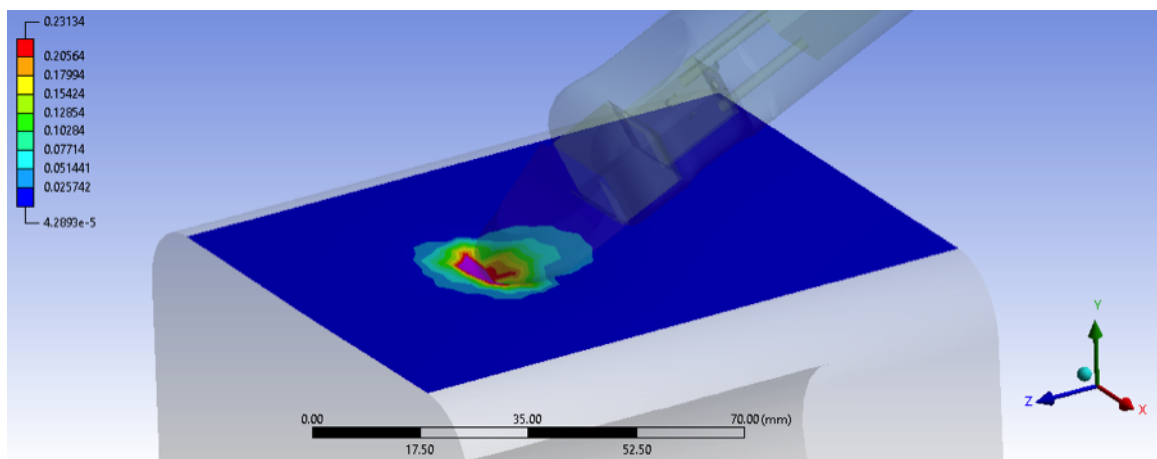


Fig. 3.18. Maximum Equivalent Stress under Hand Pressure of 0.20 MPa (Frictional Connection)

increases when hand pressure is applied, too. Although the compression stress on skin is slightly higher than the tension stress, which was recorded when hand pressure increased to 0.25 MPa, as shown in Figure 3.20.

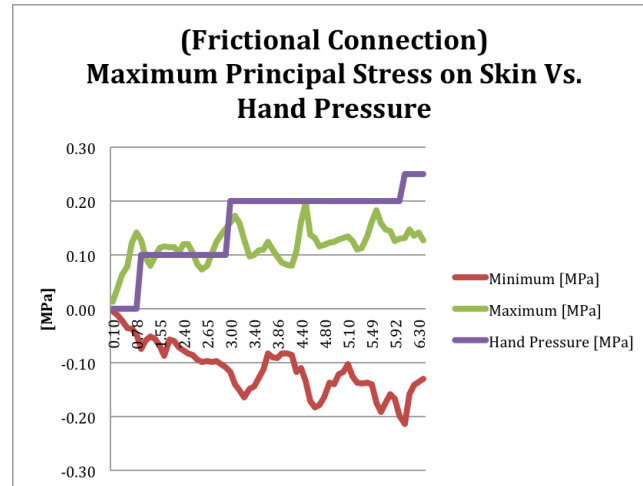


Fig. 3.19. Maximum Principal Stress on Skin vs. Hand Pressure (Frictional Connection)

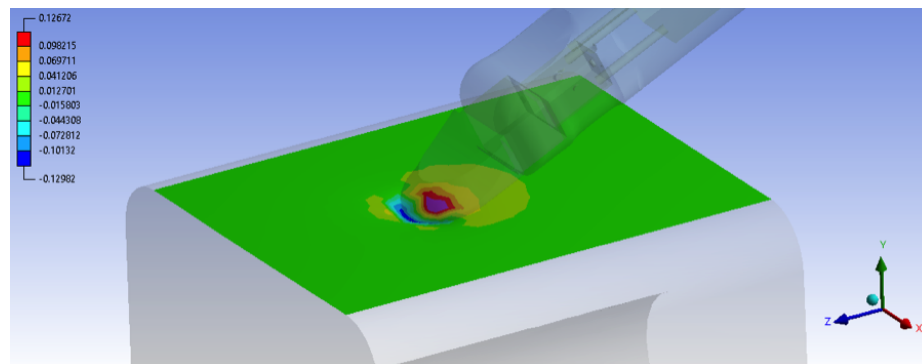


Fig. 3.20. Maximum Value of the Maximum Principal Stress Under Hand Pressure of 0.25 MPa (Frictional Connection)

Skin/tissue deformation is an important factor in IASTM process in order to ensure the optimal treatment of the restricted tissues. As shown in Figure 3.21, the maximum and minimum deformation values reached their maximum after the hand pressure increased to 0.25 MPa at 6.2 second with 4.0012 mm and 0.18247 mm, respectively. To visualize the maximum total deformation, a photograph has been taken at that moment, as shown in Figure 3.22.

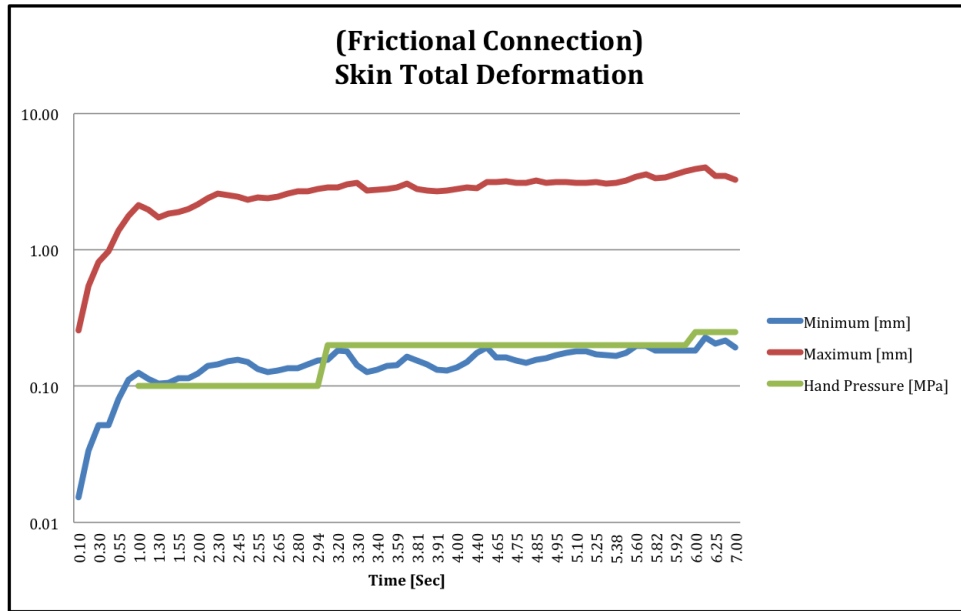


Fig. 3.21. Skin Total Deformation (Frictional Connection)

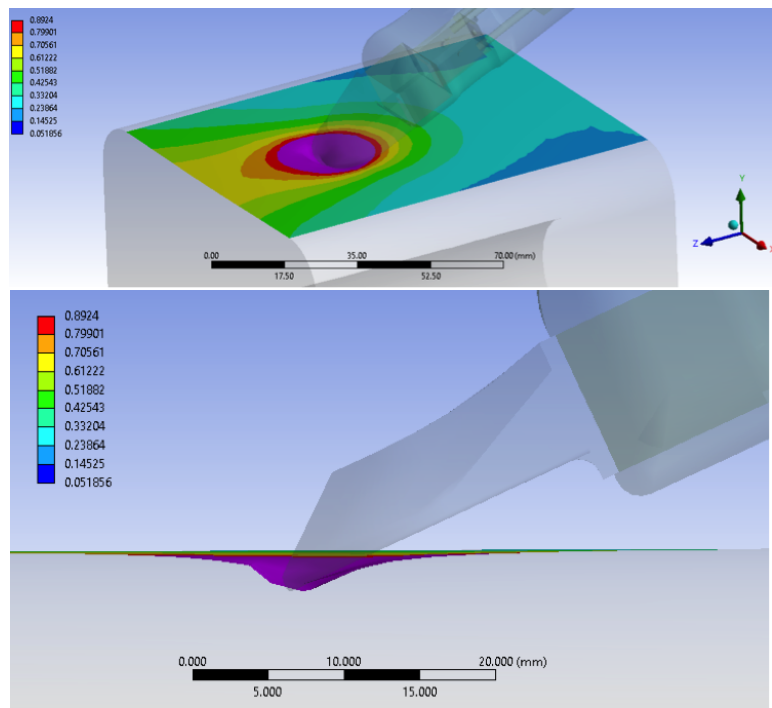


Fig. 3.22. Maximum Total Deformation (4.0012 mm) Under Hand Pressure 0.25 MPa (Frictional Connection)

IASTM Force Simulation Results

The force measurements have been investigated when the IASTM device interacted with the patients arm model at an angle of 20 degrees in ANSYS Workbench, to show the force/stress levels at the load cell tips ($Area = 2mm^2$) in relation to the therapists hand force. As shown in Figure 3.23, the maximum stress on the load cells measurement has been exported, where stress measurements have been recorded on each load cells tip. The maximum stress measurements by F+y and Fz recorded a higher stress than the stresses on the X axis load cells, because the device is rotated only around the pitch angle of 20 degrees and that agrees with the vector analysis that has been discussed before. The maximum stress measured by F+y was relatively smaller than the measured stress in Fz until the hand pressure increased to 0.20 MPa and the skin deformed 2.8566 mm. As a result, F+y load cell will measure a slightly higher value than Fz when the hand pressure and skin deformation increases.

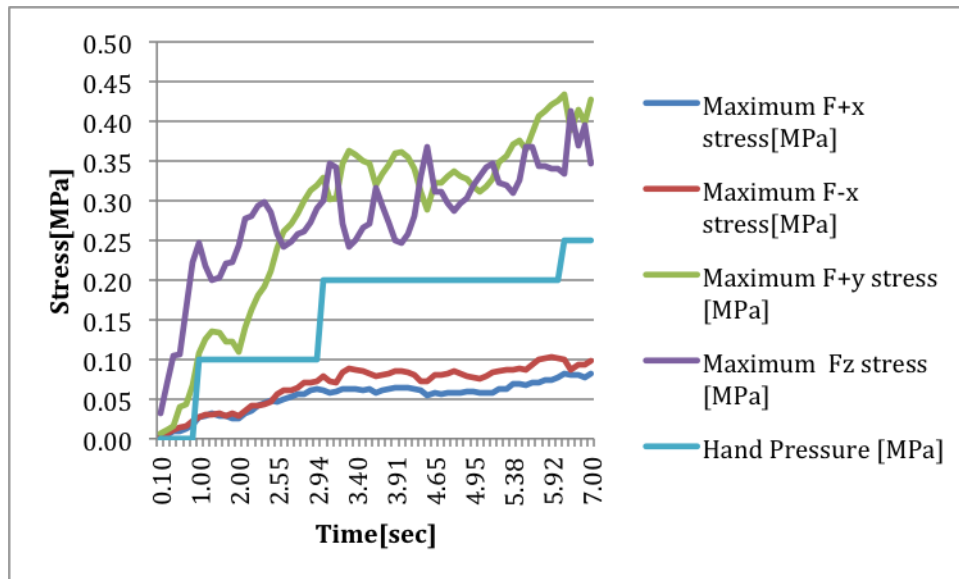


Fig. 3.23. Maximum Four Load Cells Stress Distribution vs. hand pressure (Frictional Connection)

On the other hand, the minimum stresses recorded in the directions F+y and FZ were large after increasing the hand pressure to 0.20 MPa with resulting skin

deformation of 2.8566 mm, as shown in Figure 3.24. However, stress measurement in the X axis is still low but not higher than the maximum values.

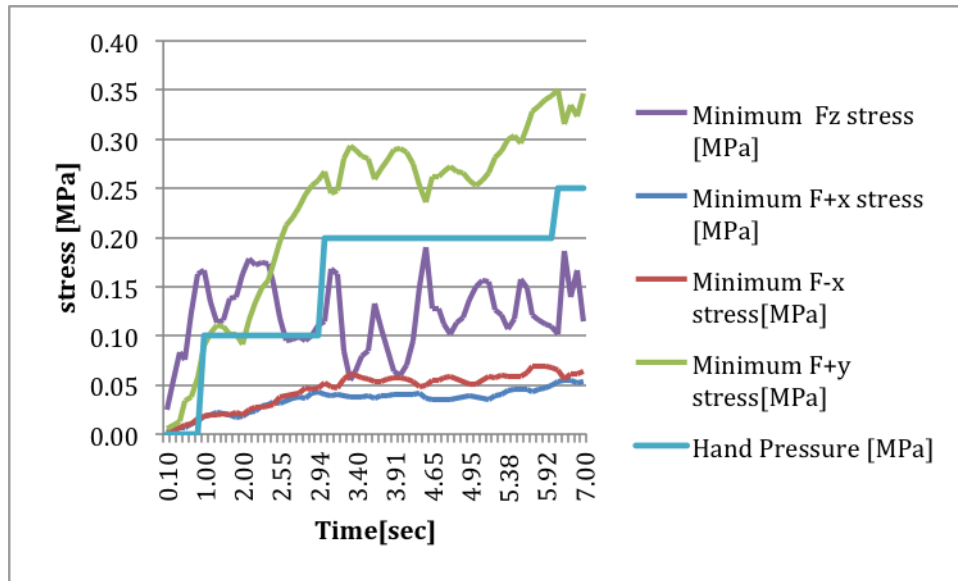


Fig. 3.24. Minimum Four Load Cells Stress Distribution vs. Hand Pressure (Frictional Connection)

3.2.2 Bonded Scenario

The simulation was successfully solved to compute the desired stresses and strains on different components, which resulted from the hand force applied by a therapist, using ANSYS Workbench R15.0. The following subsections explore the relationship between stress and deformation on the skin, and the simulation of the measured forces by the load cell's tips.

Simulated Skin Results

As shown in Figure 3.25, the relationship between the Von Mises Stress (Equivalent Stress) and hand pressure was generated using ANSYS Workbench. It's clear that the maximum and minimum Equivalent Stress were proportional to the hand

force. In terms of maximum Equivalent Stress, the maximum value was recorded at the maximum hand force (120 N), as shown in Figure 3.26. To reduce the scope, the base 10 logarithm was used to generate the graph. The minimum value was approximately zero during the simulation.

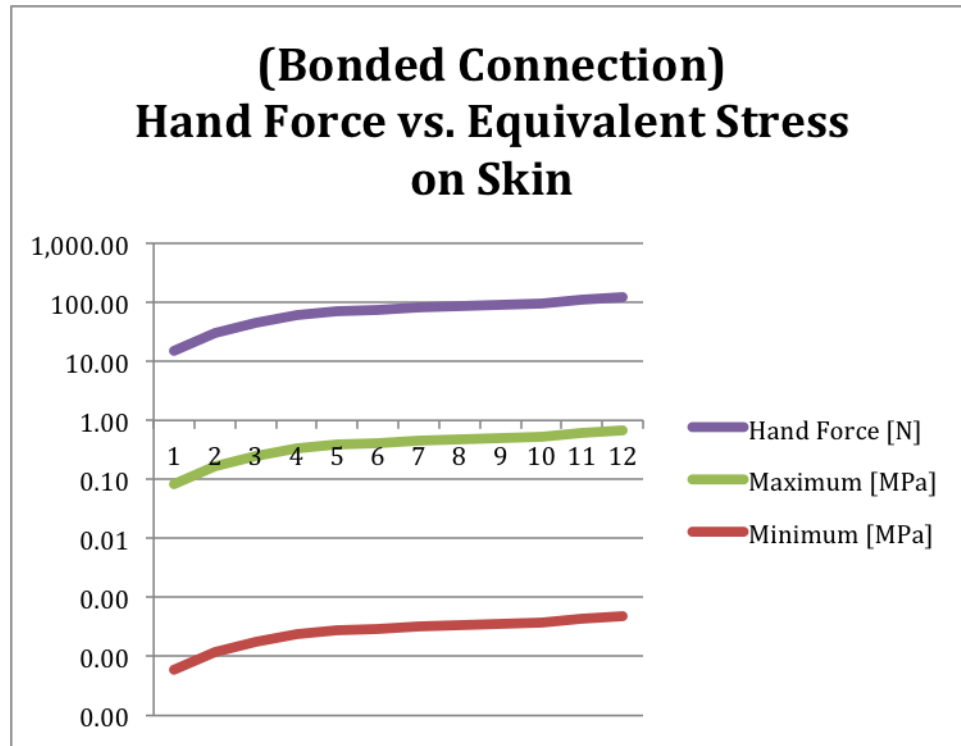


Fig. 3.25. Hand Force vs. Equivalent Stress on Skin (Bonded Connection)

The relationship between the minimum and maximum readings for the Maximum Principal Stress was generated, as shown in Figure 3.27. The maximum and minimum values of the Maximum Principal Stress were proportional to the hand force, and they represent the tension and compression stresses on skin, respectively. The compression stress on skin was slightly higher than the tension stress, which was recorded when the hand force reached 100 N, as shown in Figure 3.28.

In terms of skin/tissue deformation, the maximum and minimum deformation values reached their maximum when the hand force reached 120 N, 9.2811 mm and

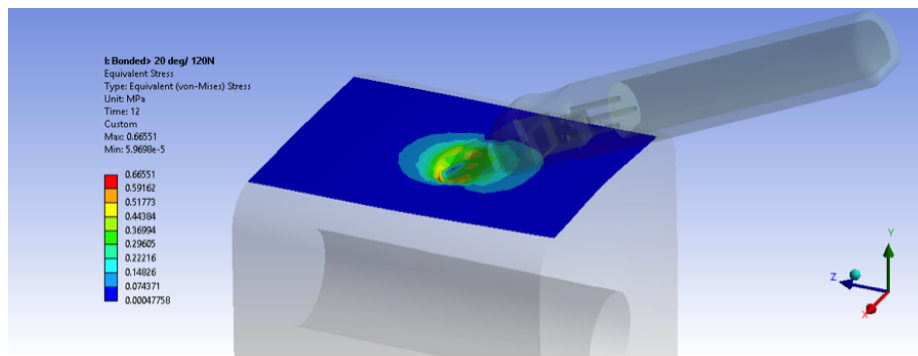


Fig. 3.26. Maximum Equivalent Stress under Maximum Hand Force (120 N) (Bonded Connection)

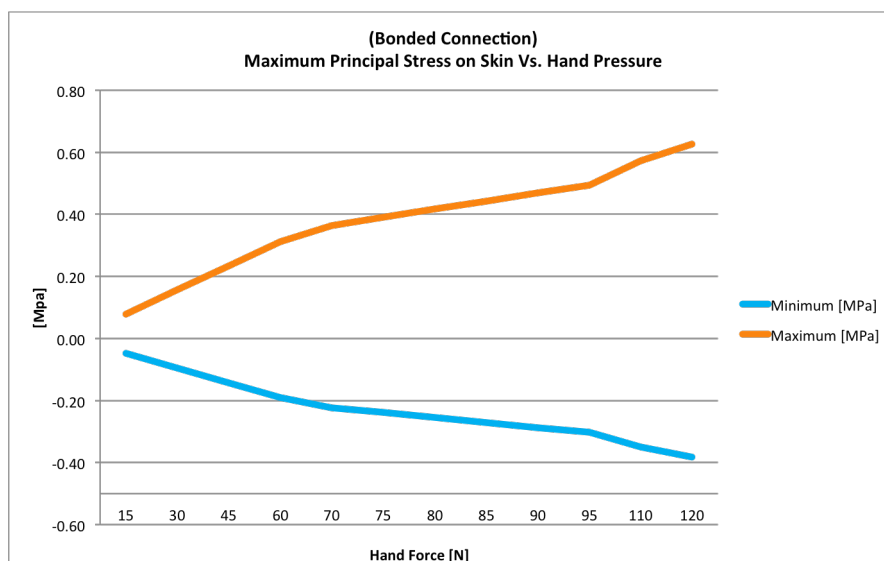


Fig. 3.27. Maximum Principal Stress on Skin vs. Hand Force (Bonded Connection)

1.4865 mm, respectively, as shown in Figure 3.29. To visualize the maximum total deformation, an image was recorded at that moment, as shown in Figure 3.30.

IASTM Force Simulation Results

The force measurements were investigated when the IASTM device interacted with the patient's arm model at an angle of 20 degrees in ANSYS Workbench, to show the

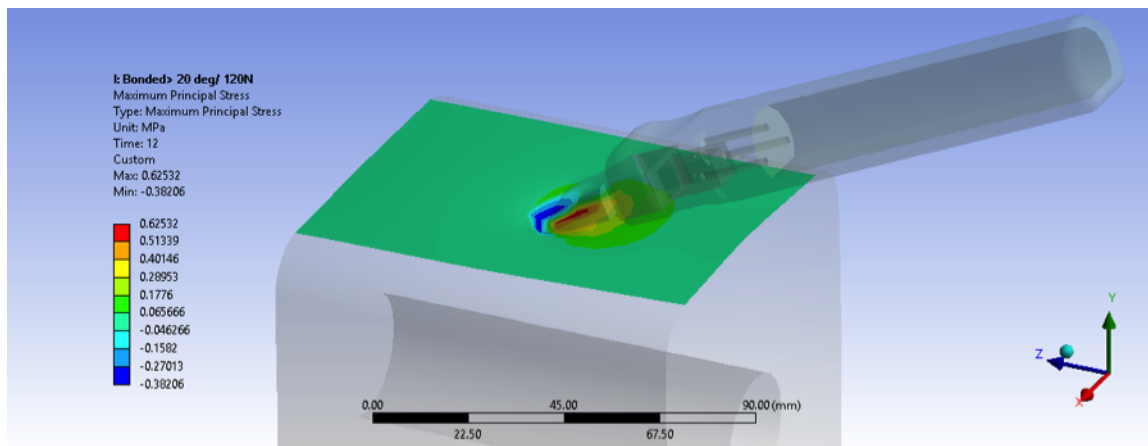


Fig. 3.28. Maximum Value of the Maximum Principal Stress Under Maximum Hand Force (120 N) (Bonded Connection)

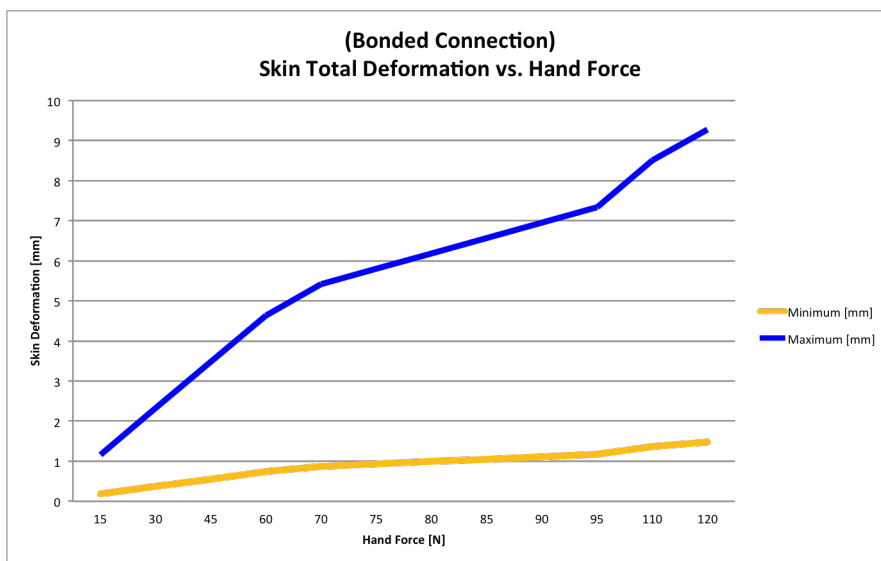


Fig. 3.29. Skin Total Deformation (Bonded Connection)

force/stress levels at the load cells tips ($Area = 2mm^2$) in relation to the therapists hand force. As shown in Figure 3.31 and 3.32, the maximum and minimum stresses on the load cells measurement were exported, where stress measurements were recorded on each load cells tip. The maximum and minimum stress measurements of load

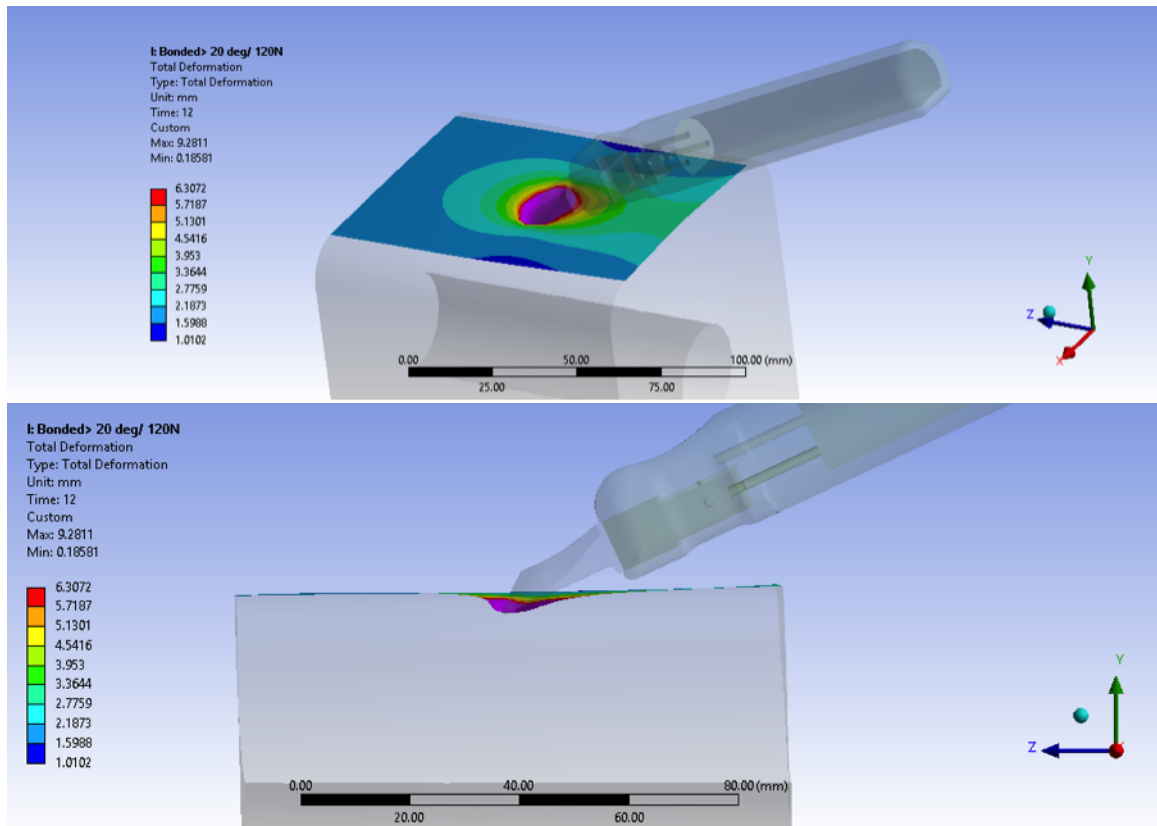


Fig. 3.30. Maximum Total Deformation Under Hand Force 120 N

cells $F+y$ and Fz were higher than the stresses on the X axis's load cells, because the device was rotated around the pitch angle of 20 degrees, which agreed with the vector analysis that was discussed before. The stress on load cell Fz was measured at the highest maximum and minimum stress/force during the complete simulation, followed by $F+y$.

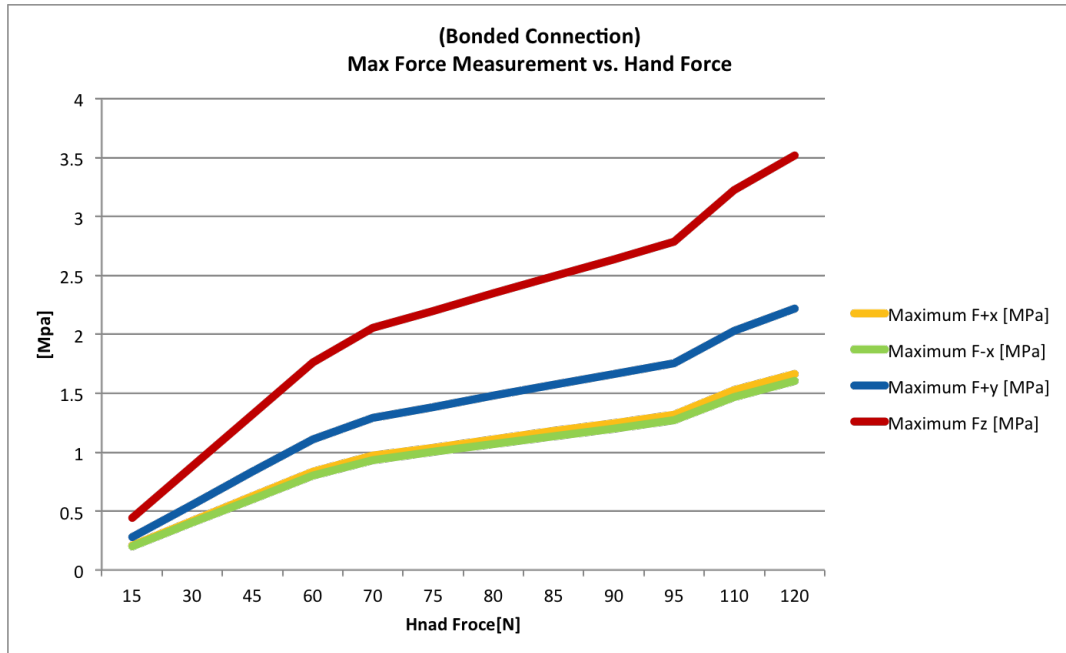


Fig. 3.31. Maximum Four Load Cells' Stress Distribution vs. Hand Force

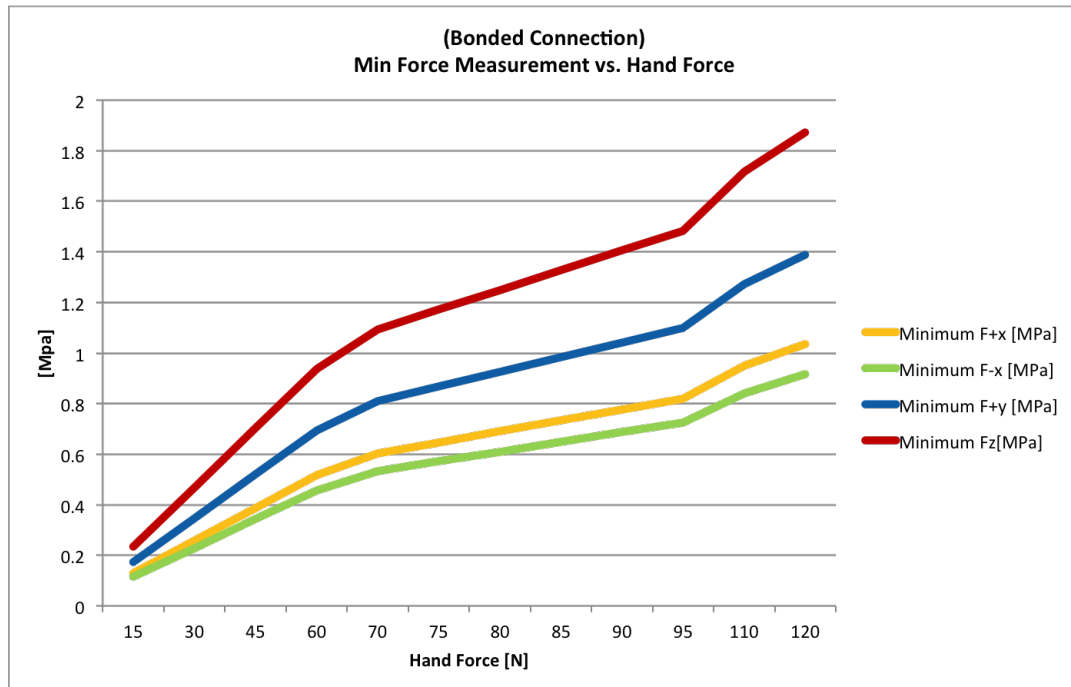


Fig. 3.32. Minimum Four Load Cells' Stress Distribution vs. Hand Pressure

4. MEASUREMENTS VALIDATION TEST

4.1 Validation Systems

After the 3D compression load cell based IASTM device was assembled, validation tests were performed to check the measurements accuracy and repeatability. The IASTM technique is used to enhance the restricted tissue by applying a certain amount of force and angle, which must be quantified accurately. And that will allow the new IASTM device to standardize the IASTM practice and move it to the next level, which is human study.

4.1.1 Force Validation System

A validation system was built to insure that the IASTM device met the force measurement requirements. The system was based on electronic scale (PCE-PB 150N) with readability of 0.01 N to measure the vertical force component on the scale plate, as shown in Figure 4.1 . Different weights placed on the scale to check the scale accuracy. As shown in Table 4.1, the scale couldn't detect any load less than 100 g. However, the absolute relative error varied between 0 and 2.06 % for the rest of load measurements.



Fig. 4.1. Electronic Scale

Table 4.1
Summary of The Scale Accuracy Test

The Scale Accuracy			
Weight (g)	Scale Measured		Relative Error %
	Gram (g)	Newton (N)	
50.00	0.00	0.00	-100.00
100.00	0.00	0.00	-100.00
150.00	150.00	1.50	0.00
200.00	200.00	2.00	0.00
250.00	250.00	2.50	0.00
300.00	300.00	3.00	0.00
350.00	350.00	3.50	0.00
400.00	400.00	4.00	0.00
1019.72 (10N)	1000.00	10.00	-1.93
1369.72 (10N+350)	1350.00	13.00	-1.44
1419.72 (10 N+400)	1400.00	13.50	-1.39
1469.72 (10N +450)	1500.00	14.50	2.06

The scale measurement in Newtons was acquired using Labview software through a serial port interface. According to the scale manufacturer (Appendix C), the scale measurement is transferred in 16 digits using the scale controller through a USB cable,

as shown in Table 4.2. The scale measurement is placed between the third and tenth byte, where the second and eleventh bytes are spaces and the measurement unit is stored in bytes 13 and 14. As a result, a Labview model was constructed to extract the scale measurement based on the previous criteria, as shown in Figure 4.2. The scale measurement was embedded into the main IASTM device using the Labview model to provide the user with all measurements in one display.

Table 4.2
Scale Data Format

Digit	1	2	3	4	5	6	7	8	9	10	11	12	13	14	15	16	
Data	⌘	Space	Measured Value							Space	-	Unit	CR	LF			

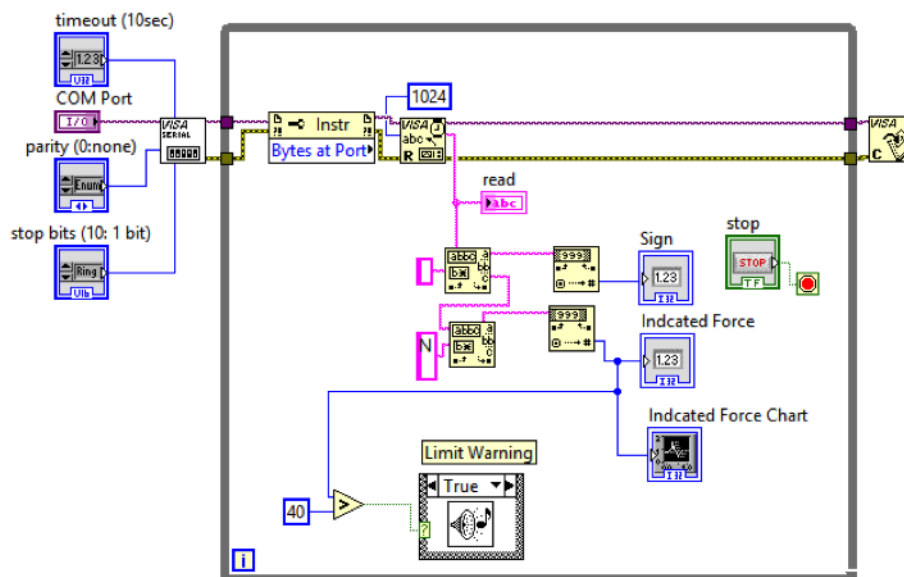


Fig. 4.2. Scale Labview Model

4.1.2 Angle Validation System

A validation system was built to insure that the IASTM device met the angle measurement requirements. As shown in Figure 4.3, the combination square set was set on flat surface.

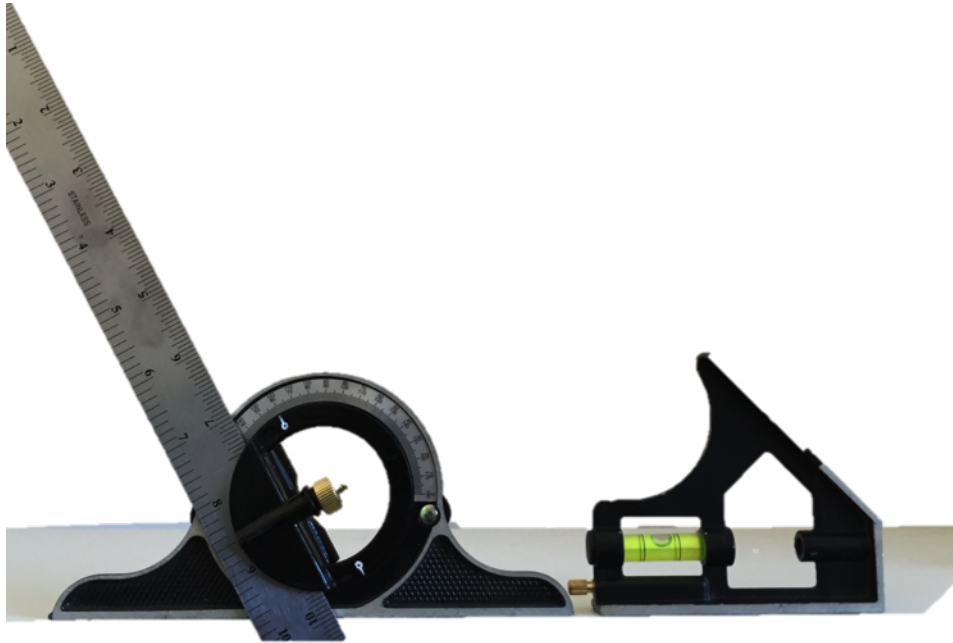


Fig. 4.3. Combination Square Set (Angle Validation System)

4.2 Methodology and Test Results

Three student examiners from the School of Health and Rehabilitation Science at IUPUI were assigned to use the new IASTM device and apply force to the scale plate with different pitch angles. In the first and second test, each student was asked to apply as much force as possible five times through the IASTM device with a pitch angle between 85 to 95 degrees (holding the device perpendicular to the scale surface) using a pencil grip hand position, as shown in Figure 4.4. The 3D load cell and scale measurements were exported. The absolute relative error varied between 0 and 5.9 %, as shown in Tables 4.3 and 4.4.

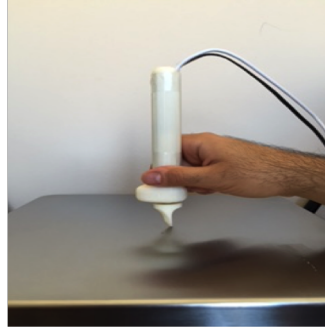


Fig. 4.4. Hand Position of IASTM Device in the First and Second Tests

Table 4.3
Summary of The First Force Measurement Test

Examiner 1		
Peak IASTM Device (N) (3D Z-Force Component)	Peak Force Plate (N)	Relative Error %
25.44	26.50	-4.00
29.80	31.50	-5.40
28.70	29.50	-2.71
25.50	26.50	-3.77
30.90	31.00	-0.32
Examiner 2		
Peak IASTM Device (N) (3D Z-Force Component)	Peak Force Plate (N)	Relative Error %
28.70	28.00	2.50
28.70	29.50	-2.71
27.70	28.00	-1.07
33.00	33.00	0.00
32.00	33.00	-3.03
Examiner 3		
Peak IASTM Device (N) (3D Z-Force Component)	Peak Force Plate (N)	Relative Error %
22.24	22.00	1.09
29.80	30.50	-2.30
28.70	30.00	-4.33
31.90	32.50	-1.85

Table 4.4
Summary of The Second Force Measurement Test

Examiner 1		
Peak IASTM Device (N) (3D Z-Force Component)	Peak Force Plate (N)	Relative Error %
33.10	32.00	3.44
25.50	25.00	2.00
28.80	28.00	2.86
28.70	28.50	0.70
Examiner 2		
Peak IASTM Device (N) (3D Z-Force Component)	Peak Force Plate (N)	Relative Error %
27.70	27.00	2.59
27.70	28.00	-1.07
29.80	29.00	2.76
27.70	28.50	-2.81
29.80	31.00	-3.87
Examiner 3		
Peak IASTM Device (N) (3D Z-Force Component)	Peak Force Plate (N)	Relative Error %
29.80	30.50	-2.30
31.90	32.00	-0.31
28.70	30.50	-5.90
29.80	30.00	-0.67
28.70	29.50	-2.71

In the third test, each student was asked to apply as much force as possible, but the IASTM devices pitch angle had to be within 40 to 50 degrees using a pencil grip hand position, as shown in Figure 4.5. An exercise mat was inserted between device's tip and scale plate to simulate skin behavior. The 3D load cell and scale measurement were exported. The absolute relative error varied between 2.74 and 11.43 %, as shown in Table 4.5. The maximum absolute relative error was higher than previous test because of the existence of the exercise mat. These test results indicated the IASTM device had great repeatability and accuracy criteria.

In terms of angle measurement, the IASTM device was attached to a ruler arm of the combination square set at three different angles, 30, 45 and 60 degrees, as shown in

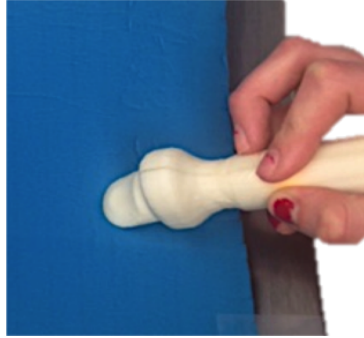


Fig. 4.5. Hand Position of IASTM Device in the Third Test

Table 4.5
Summary of The Third Force Measurement Test

Examiner 1		
45° Peak IASTM Device (N) (3D Z-Force Component)	45° Peak Force Plate (N)	Relative Error %
4.84	5.00	-3.20
5.32	5.50	-3.27
3.86	3.50	10.29
3.10	3.50	-11.43
Examiner 2		
45° Peak IASTM Device (N) (3D Z-Force Component)	45° Peak Force Plate (N)	Relative Error %
10.60	11.00	-3.64
9.95	9.00	10.56
8.29	7.50	10.53
7.43	7.70	-3.51
10.00	9.00	11.11
Examiner 3		
45° Peak IASTM Device (N) (3D Z-Force Component)	45° Peak Force Plate (N)	Relative Error %
8.27	8.00	3.37
9.76	9.50	2.74
9.53	9.00	5.89
7.09	6.50	9.08
8.10	9.00	-10.00

Figures 4.6, 4.7 and 4.8, respectively. The indicated pitch angle from the combination square set and the measured pitch angle from the Labview were compared, as shown in Table 4.6. The absolute relative error varied between 1.6 and 3.3 %. The angle test results indicated that the IASTM device had an accurate pitch angle measurement.

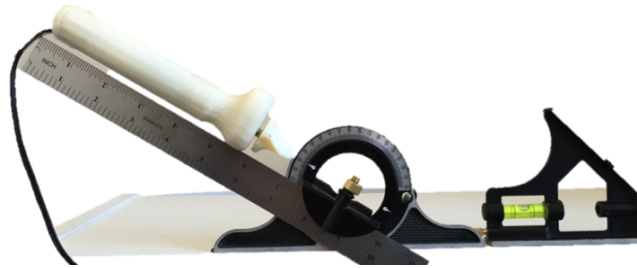


Fig. 4.6. IASTM Device at 30 Degrees

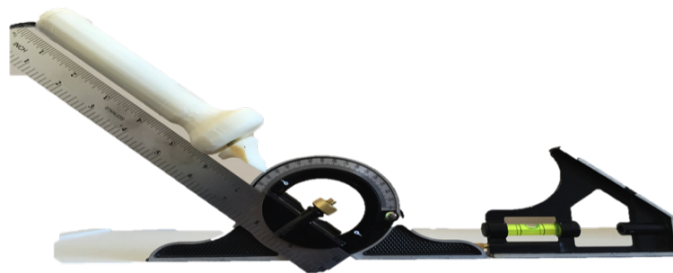


Fig. 4.7. IASTM Device at 45 Degrees

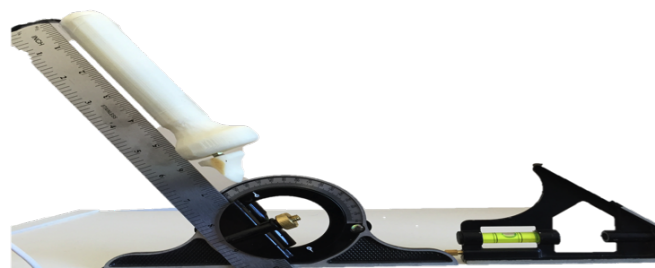


Fig. 4.8. IASTM Device at 60 Degrees

Table 4.6
Summary Pitch Angle Measurement Test

Indicated Pitch Angle	Measured Pitch Angle	Relative Error %
30 Degrees	29 Degrees	-3.33
45 Degrees	46 Degrees	2.22
60 Degrees	61 Degrees	1.6

4.3 IASTM Device Dynamic Analysis

After force and angle measurements were proven to be effective and accurate, the IASTM device' measurement systems were connected to examine and analyze the complete device. An examiner was asked to apply a random number of force strokes to skin with an approximated pitch angle of 45 degrees. As shown in Figure 4.9, the Fz and Fy force components on the skin surface (skin coordinate) were almost identical during the test time, which was 21.5 seconds, because the pitch angle was approximately 45 degrees and that would distribute the applied force equally for the Fz and Fy components. The examiner attempted to maintain the device at 45 degrees during the test, however, every time the IASTM device interacted with the skin, the examiners hand tilted the device to approximately 50 degrees.

As illustrated before, the stroke counter was based on the beak detector of the untransformed force component in the Z direction at the 3D compression load cell center. The Labview front panel indicated that the examiner delivered 17 pressure strokes to the skin; however, the examiner delivered 18 strokes based on the examiner count and untransformed Fz reading, as shown in Figure 4.10. As a result, the stroke counter was accurate with an absolute relative error of 5.5 %.

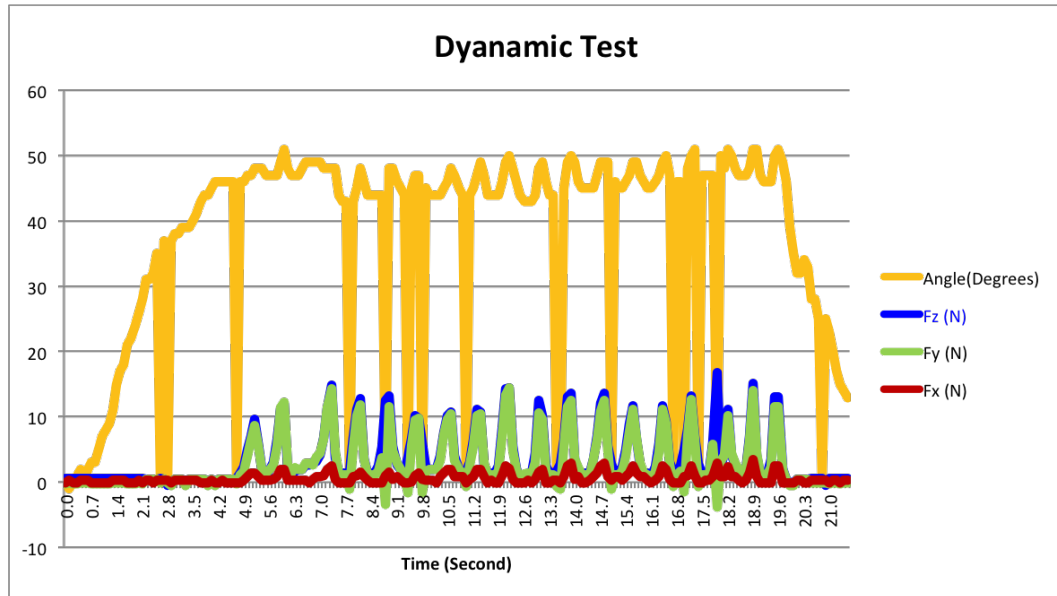


Fig. 4.9. Summary of the Dynamic Test for the IASTM Device

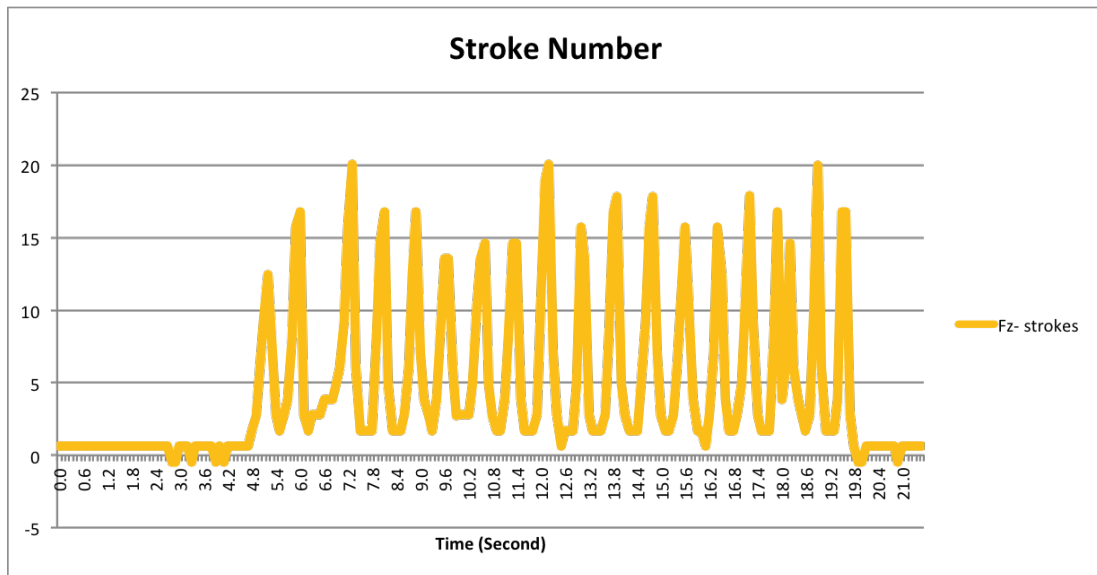


Fig. 4.10. Stroke Number During the Dynamic Test

5. CONCLUSION AND FUTURE WORK

5.1 Conclusion

Instrument assisted soft tissue mobilization (IASTM) is a form of massage using rigid manufactured or cast devices. The delivered force, which is a critical parameter in the massage during IASTM, has not been objectively measured or standardized for clinical practices. In addition to force magnitude, the angle of treatment and frequency play an important role during IASTM. There is a strong need to characterize the delivered force to a patient, angle of treatment, and stroke frequency. In this thesis, two novel devices were developed to deliver localized pressure to the soft tissue. The first design was compression load cell based, where four load cells were used to measure the three force components in three-dimensional space.

A finite element analysis using Ansys software was created for the 1D compression load cell based device to simulate IASTM practice using the IASTM device, which was based on the 1D compression load cells. Bonded and frictional scenarios, which were based on the relationship between the device tip and skin model, were simulated. Deformation and stress on the skin were measured after applying a certain amount of force with the GT-3 tool. In addition, the relationship between skin stress and the load cell measurements were investigated.

Both design were used an IMUduino microcontroller board to measure IASTM orientation angles and stroke frequency. The second design, which was based on a 3D load cell, could measure all three component forces by itself, and measurements were transferred to a portable laptop using a data acquisition card from National Instruments. The force measurements were transferred and represented with respect to the skin coordinate system based on the orientation angles and the distance between the device's tip and the load cell placement. LABVIEW software was used to program

and display all required measurements in a user-friendly interface. Orientation angles and stroke frequency were measured by an IMUduino microcontroller, similar to the first design.

In terms of validation, an electronic plate scale was used to measure known applied forces. The load cell measurements and the scale reading were compared to determine the accuracy of the IASTM device. The absolute relative error varied between 0 and 11 %. The angle measurement was tested using a combination square set tool, and the absolute relative error varied between 0 and 3.3 %. The IASTM device was tested to collect and examine the device performance. The device was found to be accurate and stable during real dynamic operation mode.

5.2 Future Work Recommendation

The findings in this thesis suggest several possible future projects. First, the device should be tested for reliability using a small animal model prior to use in humans. Next, the design concepts could be expanded to different shaped treatment device tips to allow for contoured treatment of different body regions. Also, a finite element simulation could be created for the second design to simulate IASTM practice using the IASTM device; different angles and device movements could be simulated to investigate the force measurement for both devices. Pencil grip position for the 1D compression load cell can be investigated, too. In addition, the angle measurement code could be modified to include different orientation angles with respect to different treatment surface inclinations using quaternion coordinate. Stroke length can be measured using a laser displacement sensor, which might be fixed on the device's tail or an external frame next to the treatment surface. The resonance, which impacts the tissue rehabilitation progress, can be quantified using a piezo vibration sensor maintained inside device's tip.

LIST OF REFERENCES

LIST OF REFERENCES

- [1] S. Kumar, K. Beaton, and T. Hughes, “The effectiveness of massage therapy for the treatment of nonspecific low back pain: A systematic review of systematic reviews,” 2013.
- [2] J. D. Crane, D. I. Ogborn, C. Cupido, S. Melov, a. Hubbard, J. M. Bourgeois, and M. a. Tarnopolsky, “Massage therapy attenuates inflammatory signaling after exercise-induced muscle damage,” *Science Translational Medicine*, vol. 4, no. 119, pp. 13–119, 2012.
- [3] T. M. Best, S. K. Crawford, C. Haas, L. Charles, and Y. Zhao, “Transverse forces in skeletal muscle with massage-like loading in a rabbit model,” *BMC Complementary and Alternative Medicine*, vol. 14, pp. 1–9, 2014.
- [4] C. J. Davidson, L. R. Ganion, G. M. Gehlsen, B. Verhoestra, J. E. Roepke, and T. L. Sevier, “Rat tendon morphologic and functional changes resulting from soft tissue mobilization.,” *Medicine and science in sports and exercise*, vol. 29, no. 3, pp. 313–319, 1997.
- [5] G. M. Gehlsen, L. R. Ganion, and R. Helfst, “Fibroblast responses to variation in soft tissue mobilization pressure.,” *Medicine and science in sports and exercise*, vol. 31, no. 4, pp. 531–5, 1999.
- [6] M. T. Loghmani and S. J. Warden, “Instrument-assisted cross-fiber massage accelerates knee ligament healing.,” *The Journal of orthopaedic and sports physical therapy*, vol. 39, no. 7, pp. 506–514, 2009.
- [7] M. T. Loghmani and S. J. Warden, “Instrument-assisted cross fiber massage increases tissue perfusion and alters microvascular morphology in the vicinity of healing knee ligaments,” *BMC Complementary and Alternative Medicine*, vol. 13, p. 1, 2013.
- [8] B. Looney, T. Srokose, C. Fernandez-De-Las-Peas, and J. A. Cleland, “Graston instrument soft tissue mobilization and home stretching for the management of plantar heel pain: A case series,” *Journal of Manipulative and Physiological Therapeutics*, vol. 34, no. 2, pp. 138–142, 2011.
- [9] A. J. Bayliss, F. J. Klene, E. L. Gundeck, and M. T. Loghmani, “Treatment of a patient with post-natal chronic calf pain utilizing instrument-assisted soft tissue mobilization: a case study,” *Journal of Manual & Manipulative Therapy*, vol. 19, no. 3, pp. 127–134, 2011.
- [10] E. C. McCrea and S. Z. George, “Outcomes following augmented soft tissue mobilization for patients with knee pain: a case series.,” *Orthopaedic Physical Therapy Practice*, vol. 22, no. 2, pp. 69–74, 2010.

- [11] J. Burke, D. J. Buchberger, M. T. Carey-Loghmani, P. E. Dougherty, D. S. Greco, and J. D. Dishman, "A pilot study comparing two manual therapy interventions for carpal tunnel syndrome," *Journal of Manipulative and Physiological Therapeutics*, vol. 30, no. 1, pp. 50–61, 2007.
- [12] G. TECHNIQUE, "History of graston technique," 2016. [Online]. Available: <http://www.grastontechnique.com/history>. [Accessed: 21- Feb- 2016].
- [13] G. TECHNIQUE, "Graston technique advantages," 2016. [Online]. Available: <http://www.grastontechnique.com/home>. [Accessed: 21- Feb- 2016].
- [14] R. L. Phipps, S. R. Carney, M. T. Loghmani, and A. J. Bayliss, "Title: An innovative manual therapy approach for the treatment of patients with achilles tendinopathy: A case series," *Journal of orthopaedic and sports physical therapy*, 2011.
- [15] M. L. Heinecke, S. T. Thuesen, and R. C. Stow, "Graston technique on shoulder motion graston technique on shoulder motion in overhead athletes," *Journal of Undergraduate Kinesiology Research*, vol. 1, no. 10, pp. 27–39, 2014.
- [16] K. Laudner, B. D. Compton, T. A. McLoda, and C. M. Walters, "Acute effects of instrument assisted soft tissue mobilization for improving posterior shoulder range of motion in collegiate baseball players.," *International journal of sports physical therapy*, vol. 9, no. 1, pp. 1–7, 2014.
- [17] M. Terry Loghmani, A. J. Bayliss, G. Clayton, and E. Gundeck, "Successful treatment of a guitarist with a finger joint injury using instrument-assisted soft tissue mobilization: a case report.," *The Journal of manual & manipulative therapy*, vol. 23, pp. 246–53, 12 2015.
- [18] P. Black *et al.*, "Treatment of knee arthrofibrosis and quadriceps insufficiency after patellar tendon repair: a case report including use of the graston technique," *International Journal of Therapeutic Massage & Bodywork: Research, Education, & Practice*, vol. 3, no. 2, pp. 14–21, 2010.
- [19] H. M. Lee, S. K. Wu, and J. Y. You, "Quantitative application of transverse friction massage and its neurological effects on flexor carpi radialis," *Manual Therapy*, vol. 14, no. 5, pp. 501–507, 2009.
- [20] Q. Wang, H. Zeng, T. M. Best, C. Haas, N. T. Heffner, S. Agarwal, and Y. Zhao, "A mechatronic system for quantitative application and assessment of massage-like actions in small animals," *Annals of biomedical engineering*, vol. 42, no. 1, pp. 36–49, 2014.
- [21] H. Zeng, T. A. Butterfield, S. Agarwal, F. Haq, T. M. Best, and Y. Zhao, "An engineering approach for quantitative analysis of the lengthwise strokes in massage therapies," *Journal of Medical Devices*, vol. 2, no. 4, p. 041003, 2008.
- [22] Femto.io, "Imuduino," 2016. [Online]. Available: <http://femto.io/products>. [Accessed: 21- Feb- 2016].
- [23] L. Forsentek Co., "Micro compression load cell force sensor 5kg 10kg 20kg 50kg 100kg," 2016. [Online]. Available: <http://www.forsensor.com/>. [Accessed: 21- Feb- 2016].

- [24] M. W. Spong, S. Hutchinson, and V. M., *Robot Modeling and Control*, vol. 141. 2006.
- [25] P. G. Agache, C. Monneur, J. L. Leveque, and J. De Rigal, “Mechanical properties and young’s modulus of human skin in vivo.,” *Archives for dermatological research. Archiv fur dermatologische Forschung*, vol. 269, pp. 221–232, 1980.
- [26] G. Elert, *The physics hypertextbook*, vol. 9. 1998. [Online]. Available: <http://physics.info>. [Accessed: 21- Feb- 2016].
- [27] A. Delalleau, G. Josse, J. M. Lagarde, H. Zahouani, and J. M. Bergheau, “Characterization of the mechanical properties of skin by inverse analysis combined with the indentation test,” *Journal of Biomechanics*, vol. 39, no. 9, pp. 1603–1610, 2006.
- [28] A. Gallagher, A. Ní Annaidh, K. Bruyère, *et al.*, “Dynamic tensile properties of human skin,” *International Research Council on the Biomechanics of Injury*, 2012.
- [29] N. Veijgen, M. Masen, and E. van der Heide, “A novel approach to measuring the frictional behaviour of human skin in vivo,” *Tribology International*, vol. 54, pp. 38–41, 2012.
- [30] Ansys, “Introduction to contact (ansys mechanical structural nonlinearities),” 2010. [Online]. Available: <http://www.ansys.com>. [Accessed: 21- Feb- 2016].

APPENDICES

B. ARDUINO CODE FOR ANGLE MEASUREMENT (FREE IMU-YAW-PITCH-ROLL)

B.1 Code 90 Degrees

```
#include <ADXL345.h>
#include <bma180.h>
#include <HMC58X3.h>
#include <ITG3200.h>
#include <MS561101BA.h>
#include <I2Cdev.h>
#include <MPU60X0.h>
#include <EEPROM.h>
//#define DEBUG
#include "DebugUtils.h"
#include "CommunicationUtils.h"
#include "FreeIMU.h"
#include <Wire.h>
#include <SPI.h>

int raw_values[9];
//char str[512];
float ypr[3]; // yaw pitch roll
float val[9];

// Set the FreeIMU object
FreeIMU my3IMU = FreeIMU();
```

```

void setup() {
  Serial.begin(115200);
  Wire.begin();

  delay(5);
  my3IMU.init(); // the parameter enable or disable fast mode
  delay(5);
}

```

```

void loop() {

  // my3IMU.getYawPitchRoll(ypr);

  my3IMU.getEuler(ypr);
  Serial.print("x");Serial.print(round(ypr[0]));
  Serial.print("y");Serial.print(round(ypr[1]));
  Serial.print("z");Serial.println(round(ypr[2]));
  delay(10);
  //delay=10 there is deally in labview
  //delay=50there is hight nois in labview
  //delay=20 there is deally in labview( better than 10)
  //delay=30 there is less nois in labview(still bad)
  //delay=20 there is
}

```

B.2 Code 360 Degrees

```
#include "FreeIMU.h"
```

```
#include <Wire.h>
#include <SPI.h>
    #include "I2Cdev.h"
#include <EEPROM.h>
#include <MPU60X0.h>
#include <MS561101BA.h>
    #include <HMC58X3.h>
    #include "DebugUtils.h"
float ypr[3]; // yaw pitch roll
float val[9];

// Set the FreeIMU object
FreeIMU my3IMU = FreeIMU();




void setup() {
    Serial.begin(115200);
    Wire.begin();

    delay(5);
    my3IMU.init(); // the parameter enable or disable fast mode
    delay(5);
}

void loop() {
    getEuler360deg(ypr);
    Serial.print("x");Serial.print(round(ypr[0]));
    Serial.print("y");Serial.print(round(ypr[1]));
    Serial.print("z");Serial.println(round(ypr[2]));
    delay(10);
}
```

C. SCALE DATA SHEET


10.1. Functions of the keys in adjustment menu

1. "Print / Unit"  The key allows switching between menus and alternating settings.
2. "Count / Enter" key  The key is a confirmation key, if settings shall be adopted.
3. "ZERO / TARE" key  The key enables going one step back or leaving the menu.

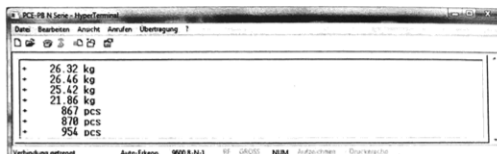
10.2 - Send

Settings of USB interface or of data transfer.

The USB interface of the scale is a bidirectional interface. Bidirectional interfaces enable a data dialogue. Thus the scale can not only send those data but also receive orders. Additionally there are several options about the exact time of sending those data to the computer. Therefore the scale provides the following transfer options:

- 10.2.1 - **KEY** Data transfer per key press, press "Print / Unit"  (approx. 2 sec.) and keep pressing until the second beep tone signals data transfer.

- 10.2.2 - **ConT** Continuous data transfer (approx. two values per second)



- 10.2.3 - **STAB** At this setting the data will only be sent, if the weighing value is steady (see stability indicator on display)



10.2.4 - ASK Data transfer on request by computer

Here the characteristics of the bidirectional interface are emphasized. By means of the following directives the scale can be remote-controlled. This allows an easy integration into systems like e.g. inventory control systems or the Delivery software of certain shipping companies like DHL, GLS etc.

- **TARE order (-T)**
This order takes the weight, which is placed on the scale
Order: ST + CR + LF

- **Enter a Tare value:**
This order allows entering a Tare value that is to subtract from the gross value.
Order: ST_ _ _ _ (respect position, compare with „enter options“)

Entering option for 60 kg scales between ST00060 and ST60180 (min. 60g / max. 60,180g)
Entering option for 150 kg scale between ST00150 and ST150450 (min. 150g / max. 150,450g)

In case the entered tare value lays above the scaling range of the scale, the display will indicate that by "****".
(The order does not function if the PEAK hold function or the function for weighing animals is activated)

- **Request for indication of current value**

Order: Sx + CR + LF

- **OFF switches off scale**

Order: SO + CR + LF

If an order is sent that the scale does not recognize, the display indicates the fault by showing "Err 5"

Interface description

Settings of the USB interface are:

Baud rate 2400 – 9600 / 8 bits / none parity / one bit stop

Format 16 digits

The display including the units ("g" / "kg" etc.) incl. the "+" or "-" digits covers a maximum of 16 digits.

Example: + 60 kg

1	2	3	4	5	6	7	8	9	10	11	12	13	14	15	16
±	SPACE	-	-	-	6	0	.	5	0	SPACE	-	k	g	CR	LF

Byte 1	-	symbol "+", "of", "-"
Byte 2	-	SPACE
Byte 3 to 10	-	number (feed-in of weight) or SPACE
Byte 11	-	SPACE
Byte 12 to 14	-	indication unit (Newton / kg / g / lb or PCS)
Byte 15	-	CR (0Dh)
Byte 16	-	LF (0Ah)

Fig. C.1. Scale Data Sheet